Uncertainty quantification of the failure assessment diagram for flawed steel components in BS 7910:2019

Maljaars, Johan; Rózsás, Árpád; Walters, Carey L.; Slot, Henk

DOI
10.1016/j.engfracmech.2022.108446

Publication date
2022

Document Version
Final published version

Published in
Engineering Fracture Mechanics

Citation (APA)
Maljaars, J., Rózsás, Á., Walters, C. L., & Slot, H. (2022). Uncertainty quantification of the failure assessment diagram for flawed steel components in BS 7910:2019. *Engineering Fracture Mechanics*, *268*, Article 108446. https://doi.org/10.1016/j.engfracmech.2022.108446

Engineering Fracture Mechanics 268 (2022) 108446

Contents lists available at ScienceDirect

Engineering Fracture Mechanics

journal homepage: www.elsevier.com/locate/engfracmech

Uncertainty quantification of the failure assessment diagram for flawed steel components in BS 7910:2019

Johan Maljaars [a,b,*], Árpád Rózsás [a], Carey L. Walters [a,c], Henk Slot [a]

[a] TNO, Stieltjesweg 1, Delft, 2628 CK, The Netherlands
[b] Eindhoven University of Technology, Groene Loper 3, Eindhoven, 5612 AE, The Netherlands
[c] Delft University of Technology, Mekelweg 2, Delft, 2628 CD, The Netherlands

ARTICLE INFO

Keywords:
Unstable fracture
Failure assessment diagram
Model uncertainty
Flawed steel structure
Probabilistic assessment

ABSTRACT

The failure assessment line (FAL) describes the interaction between plastic failure and fracture of flawed steel components subjected to tension or bending. This paper quantifies the model uncertainty of the FAL as provided in the internationally used British Standard BS 7910:2019 by comparing the assessment with the actual failure load of 82 wide plate and 4 tubular joint tests. In line with findings of others, it is demonstrated that the accuracy of the assessment is significantly improved if the crack tip constraint is considered in the assessment. Irrespective of this crack tip constraint consideration, a non-negligible number of wide plate tests has a lower failure load than the one predicted by the FAL in BS 7910:2019, if based on three fracture toughness tests. A penalty or safety margin on the FAL is advocated to compensate for this. It appears advantageous to base the assessment on the average instead of the minimum of three equivalent fracture mechanics tests together with an associated (quantified) safety margin.

1. Introduction

A flaw of a certain size in a steel structure influences the failure load. The failure mode may be related to void growth (ductile) or cleavage (brittle) fracture, depending on the material characteristics, the geometry, the loading rate, and the applied temperature. Extensive research carried out in the past has resulted in standards that describe assessment procedures for determining the acceptability of flaws in steel structures. Some of the internationally applied standards with a wide application range are BS 7910:2019 [1], API 579:2016 [2] and R6:2001 [3]. This paper focuses on [1]. An overview of the standard is given in [4]. The standard provides the failure assessment diagram for evaluating the acceptability of a flaw, see Fig. 1, where the abscissa gives the plasticity ratio, L_r, which is a measure for the proximity to plastic collapse, and the ordinate gives the fracture ratio, K_r, which is a measure for the proximity to unstable fracture. The two curves in Fig. 1 represent the Failure Assessment Lines (FAL) and they distinguish materials with or without a Lüders Plateau (LP). A flaw giving an assessment point within the bound provided by the FAL is acceptable, whereas a flaw resulting in an assessment point outside the FAL is unacceptable.

The assessment procedures and FAL have been developed as an acceptability criterion, not as a quantification of the proximity to failure [5]. To achieve this, the assessment procedures for K_r and L_r are traditionally determined such that fracture tests on large scale components fail outside of the FAL [6,7]. Yet, the procedure is also adopted in probabilistic assessments, for determining structural reliability [8], the safety on flaw size [9], or the derivation of (partial) safety factors on fracture toughness and applied stress [10,11]. Such analyses require the quantification of the difference between the predicted load at which the assessment falls

* Corresponding author at: Eindhoven University of Technology, Groene Loper 3, Eindhoven, 5612 AE, The Netherlands.
E-mail address: j.maljaars@tue.nl (J. Maljaars).

https://doi.org/10.1016/j.engfracmech.2022.108446
Received 22 November 2021; Received in revised form 10 March 2022; Accepted 4 April 2022
Available online 11 April 2022

List of symbols and definitions

Abbreviations

AIC	Akaike Information Criterion
AOTE	Average Of Three Equivalent
CCT	Centre Crack Tension
CI	Confidence Interval
CJSCT	Cruciform Joint Surface Crack Tension
CPSCT	Curved Plate Surface Crack Tension
CSCT	Coverplate Surface Crack Tension
CTOD	Crack Tip Opening Displacement
DENT	Double Edge Notch Tension
ESCT	Extended Surface Crack Tension
FAL	Failure Assessment Line
HAZ	Heat Affected Zone
HCCT	Hole containing Centre Crack Tension
LP	Lüders Plateau in the standard tensile test
MOTE	Minimum Of Three Equivalent
MU	Model Uncertainty
SCF	Stress Concentration Factor
SCT	Surface Crack Tension
TJ	Tubular Joint
WP	Wide Plate

Symbols

α	Material parameter in Ainsworth's T-stress correction equation
α_1, α_2	Parameters of the Gumbel distribution
β	Reliability index
Δ	MU
δ	CTOD
δ_m	CTOD at first attainment of a maximum force plateau for fully plastic behaviour
$\mathcal{N}$	Normal distribution
μ_X	Mean of variable X
ν	Poisson ratio
Φ	Cumulative standard normal distribution
ϕ	Polar angle of the failure assessment diagram
ψ	180 minus weld flank angle, in degrees
ρ	Plasticity interaction effect
σ_X	Standard deviation of variable X
θ	Temperature
ζ	Equivalent crack size
a	Crack depth in SCT specimens or (semi) crack length in other specimen types
A_ψ	Factor in the weld flank angle equation
a_d	Detected crack size
a_r	Distance between edge of rivet head and edge of rivet hole
B	Thickness
c	Semi crack length in a SCT specimen
D	Hole diameter
d_i	Radial distance between the true failure point and the FAL of specimen i

onto the FAL and the actual failure load of real structures, which is often referred to as the Model Uncertainty (MU) of the FAL. Hence, several studies have been published where Wide Plate (WP) tests subjected to tension or cylinders subjected to internal pressure were compared with the FAL to establish the MU distribution. The MU is usually expressed as the relative distance of the

E	Young's modulus
$F(s)$	Cumulative distribution function of the applied stress
f_ψ	Weld flank angle correction factor
f_w	Specimen width correction factor
g	Limit state function
k	Material parameter in Ainsworth's T-stress correction equation
K_I	Mode I stress intensity factor
K_r	Fracture ratio
K_{IC}	Plane strain fracture toughness
$K_{mat\delta}$	Fracture toughness following from the CTOD test
K^c_{matB}	Crack tip constraint corrected fracture toughness for a crack length equal to the CTOD specimen thickness
K_{mat}	Fracture toughness
K^c_{mat}	Crack tip constraint corrected fracture toughness
K_{sb}	Self balancing part of residual stress
L	Distance between weld toes
l	Effective crack front length
l_{cf}	Crack front length
l_{max}	Maximum crack front length
L_r	Plasticity ratio
$L_{r,max}$	Limit value of the plasticity ratio
m	Strength dependent $\delta - K_{mat}$ conversion factor
$M_{a,i}$, $M_{a,o}$	Applied in plane, out-of-plane bending moment on the chord in a TJ
$M_{c,i}$, $M_{c,o}$	Resistance for in plane, out-of-plane bending of the chord in a TJ
M_k	Weld toe correction factor
M_{km}, M_{kb}	Weld toe correction factor for membrane stress, for bending stress
M_m, M_b	Flaw correction factor, for membrane stress, for bending stress
P_a	Applied axial force on the chord in a TJ
P_c	Resistance for axial force of the chord in a TJ
P_u	Failure load
R	Probabilistic FAL of Dijkstra
$r_{F,i}$	Radial distance of the true failure point in the failure assessment diagram for specimen i
$r_{FAL,i}$	Radial distance of the FAL for specimen i
s	Stress
s_b	Bending stress
$s_{b,res}$	Welding residual bending stress
s_m	Membrane stress
$s_{m,res}$	Welding residual membrane stress
s_{ref}, $s_{ref\delta}$	Reference stress, reference stress in the CTOD test
s_u	Tensile strength at test temperature
s_u^{RT}	Tensile strength at room temperature
s_y	Yield stress at test temperature
s_y^{RT}	Yield stress at room temperature
T_δ	T-stress in the CTOD specimen
T_{WP}	T-stress in the WP or TJ specimen
W	Width in a WP test or height in a CTOD test
Y	Geometric correction factor

test assessment point to the FAL. Dijkstra [12] derived the MU using the assessment procedures in the guideline PD 6493:1980 [13], which is a predecessor of BS 7910 [1]. He expressed the FAL as a circle [8], see Fig. 2a:

$$R^2 = K_r^2 + L_r^2 \tag{1}$$

where R is normally distributed with a mean of $\mu_R = 1.7$ and a standard deviation of $\sigma_R = 0.4$. This model and MU distribution are included in the JCSS probabilistic model code [14]. Fig. 2(a) provides the mean and the 90% two-sided Confidence Interval (CI) of Dijkstra's FAL and the tests on which it is based.

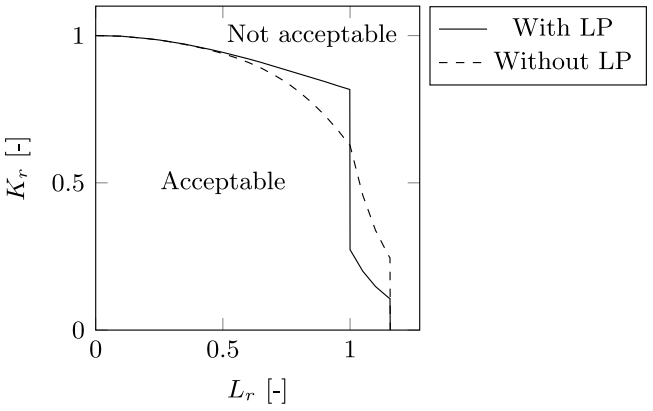

Fig. 1. Failure assessment diagram of BS 7910 [1].

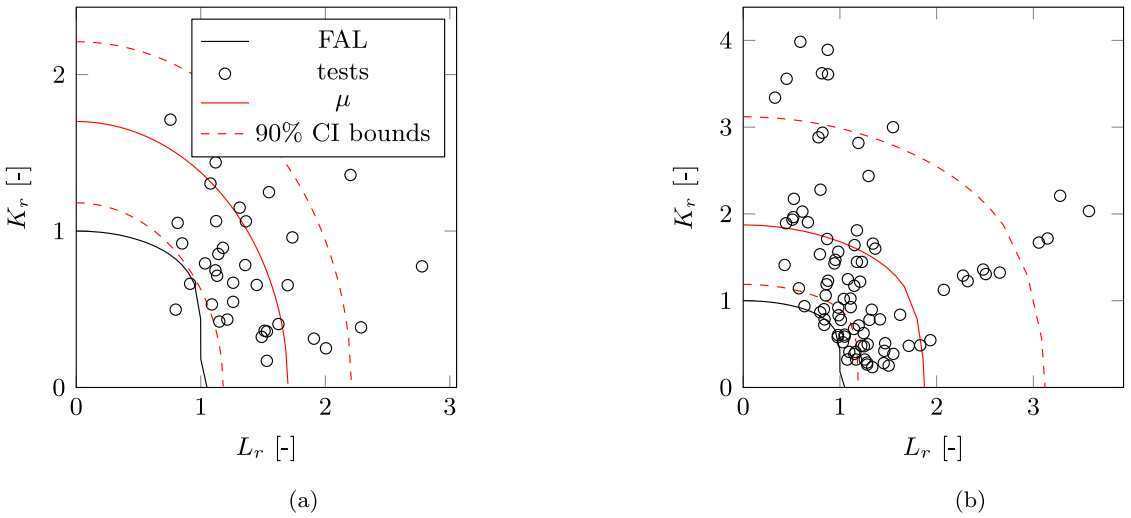

Fig. 2. MU of the FAL as determined by others (data digitalized from original papers — note: axes of subfigures have different scales): (a) Dijkstra [12] using PD 6493:1980 [13] ("modern" FAL added for reference); (b) Muhammed [15] using PD 6493:1991 [16].

Whereas Dijkstra replaced the deterministic FAL by Eq. (1), Muhammed et al. [15] used the FAL of the subsequent version PD 6493:1991 [16] as a starting point, and formulated an additive MU, i.e. the probabilistic FAL is the deterministic FAL plus the MU. Based on 90 large scale (mainly wide plate) tests, they observed a larger bias and a larger scatter for plastic collapse (low K_r) and for brittle fracture (low L_r) as compared to the interaction region. In case all data are grouped, their MU is Weibull distributed with location, scale and shape parameter of −0.06, 0.97 and 1.11, respectively, see Fig. 2b.

Burdekin and Hamour [10] have established the partial safety factors of the SINTAP/FITNET [17] fracture assessment procedures. Involving the bias and the scatter of wide plate tests in their probabilistic procedure, they determined that the partial safety factor for the applied stress can be reduced by between 0.05 and 0.1, and that the partial safety factor on fracture toughness can be reduced by between 0.2 and 1.0, compared to the case where they took the FAL as deterministic. However, they note that these reductions apply only provided the service conditions of the assessment are similar to the conditions of the wide plate tests that were used to establish the factors. Different assumptions made for the distributions of the variables cause the partial safety factors for fracture toughness recommended in different guidelines to vary widely [18].

The procedures in BS 7910:2019 [1] have been developed over decades. The current version is based on predecessors back to the previously mentioned PD 6493 [13], see [19], and advantage has been taken of other standards and guidelines such as R6 [3], FITNET [17] and SINTAP [20] as well as studies that have been published in the meantime. The procedures have been updated and alternatives added, aiming at reducing excessive conservatism in the assessment. These modifications imply that the distributions of the MU in [10,12,18] as listed before are no longer applicable or are valid only for one of the alternative procedures included in the standard.

Major developments of more detailed procedures to determine L_r accommodated by BS 7910 [1] are: parametric equations for many more types of flaw as compared to its predecessors, consideration of the out-of-plane constraint (plane stress or plane strain) for

some types of flaw, and limit load solutions specific for Tubular Joints (TJ). A major development incorporated in the procedures for K_r is the consideration of crack tip constraint, accounted for through the T-stress [21,22]. Various procedures have been developed to take the T-stress into account in the calculation of K_r. Minami and co-authors [23,24] have developed a procedure which is based on the Beremin model [25], where the Weibull stress is determined with three-dimensional finite element models. This procedure is implemented in ISO 27306 [26], but not in BS 7910 [1]. The earlier work of Ainsworth and O'Dowd [27] is based on the same theory, but they applied the results of pre-computed plane strain finite element models to estimate the Weibull stress. Comparisons between these two methods are given in [24,28]. A third approximate procedure accounts for the crack tip constraint by a simple shift of the master curve, [29]. The latter two procedures are implemented in BS 7910 [1] and they will be elaborated below. Many authors have shown that these updated procedures can reduce excessive conservatism in the assessment procedure, e.g. [30,31]. However, Hadley and Horn [28] warn that adopting the crack tip constraint procedures may result in a non-conservative assessment by showing a failed WP test that was assessed inside the FAL. Pisarski [32] also emphasizes the risk of non-conservative assessments with the updated procedures in BS 7910 [1] and he recommends to use a lower bound (such as the 5% fraction) of the fracture toughness distribution in the assessment of safety critical structures instead of the usual three (accepted) fracture toughness tests. Not related to specific assessment procedures, Slatcher [33] indicates that ten fracture toughness tests are sufficient for a reasonably accurate estimate of the characteristic fracture toughness. However, the execution of many fracture tests on each steel batch used in a structure may be uneconomic for new structures and even impossible for existing structures.

This demonstrates the necessity of quantifying the MU for the updated procedures in BS 7910 [1], not only for probabilistic assessments but also to define the FAL at a certain confidence level, i.e. the acceptability criterion of the standard. This work is dedicated to determining the MU distribution based on 86 large scale tests carried out in our institute's laboratories. Emphasis is on the influence of the consideration of the crack tip constraint on the MU of the FAL. The idea behind this database selection, in addition to the full details being available for these tests, is that these tests have not been used to develop the procedures. They therefore form a good basis for validation purposes.

2. Assessment procedure

This section describes the procedures used to assess the large scale tests. It generally follows the procedures in BS 7910 [1], but with some modifications, which are explicitly mentioned below.

2.1. Tensile test properties

Some of the tensile tests were carried out at room temperature. The following equations are used to obtain the yield stress s_y and tensile strength s_u at WP test temperature θ from the room temperature values s_y^{RT} and s_u^{RT}, respectively:

$$s_y = s_y^{RT} + \frac{10^5 \text{ MPa}}{491 + 1.8\theta/^\circ\text{C}} - 189 \text{ MPa} \tag{2}$$

$$s_u = s_u^{RT}\left(0.786 + 0.242e^{\left(\frac{-\theta}{171^\circ\text{C}}\right)}\right) \tag{3}$$

In agreement with [1], Young's modulus is assumed to increase from $E = 205$ GPa at $\theta = 25\,^\circ$C to $E = 210$ GPa at $\theta = -75\,^\circ$C and Poisson's ratio is taken as $\nu = 0.3$ independent of temperature.

2.2. Fracture ratio K_r

Standard single edge notch bending specimens were employed for obtaining the fracture toughness. The critical J-integral is available for some specimen only, whereas the Crack Tip Opening Displacement (CTOD), δ, is available for all specimens. The fracture toughness $K_{mat\delta}$ is therefore estimated from δ for all tests:

$$K_{mat\delta} = \sqrt{\frac{m s_y \delta E}{1-\nu^2}} \tag{4}$$

$$m = 1.517\left(\frac{s_y}{s_u}\right)^{-0.3188} \tag{5}$$

These equations are derived from deeply notched CTOD specimens. The current test database contains CTOD specimens with notch depths of $a = 0.3W$ or $a = 0.5W$, where a is the notch depth and W is the specimen height. To evaluate the applicability of Eq. (5), $K_{mat\delta}$ is compared to the fracture toughness following from the J-integral from the specimens for which both values are available. The ratio between $K_{mat\delta}$ and the fracture toughness following from the J-integral was on average 1.01 and 0.99 for the specimens with $a = 0.5W$ and $a = 0.3W$, respectively, with both groups containing 21 tests. The standard deviations of the ratio are 0.06 and 0.09, respectively. These standard deviations are not larger than the test database on which Eq. (5) is based [34]. The equation is therefore considered applicable for the test database used here. As a comparison, the value $m = 1.5$ as often used in earlier times, gives average ratios of 0.94 and 0.92, respectively.

BS 7910 [1] provides two procedures to account for the crack tip constraint in estimating the fracture toughness. Both procedures are applied here. The first procedure is developed by Ainsworth and O'Dowd [27]:

$$K^c_{matB} = K_{mat\delta}\frac{1+\alpha\left(\frac{-T_{WP}}{s_y}\right)^k}{1+\alpha\left(\frac{-T_\delta}{s_y}\right)^k} \tag{6}$$

where α and k are material parameters, and T_{WP} and T_δ are the T-stress of the WP and of the CTOD specimen, respectively.

Note that the T-stress in deep notched CTOD specimens is usually neglected, implying that the denominator in Eq. (6) is taken as 1, but the correction is considered necessary here because of the CTOD tests with $a = 0.3W$. The T-stress for WP, TJ and CTOD specimens is determined using the parametric equations in Annex N of BS 7910 [1]. It requires the reference stress as input, which is given in Section 2.3 of this paper. BS 7910 [1] allows evaluation of the T-stress from the combination of the applied (primary) stress and the residual (secondary) stress if it is obtained from the finite element method but, using the option of the parametric equations in Annex N, it only considers the effect of the T-stress caused by primary loading. The implications of this will be shown later. Parameters α and k in Eq. (6) are taken from parametric equations based on finite element analyses by Seal and Sherry [35]. Their $3s_y$ isostress contour and Rice and Tracey [36] contour solutions are used for cleavage fracture and ductile fracture (void growth), respectively.

The second procedure applies a T-stress based shift of the master curve:

$$K^c_{matB} = 30\ \text{MPa}\sqrt{\text{m}} + \left(K_{mat\delta} - 30\ \text{MPa}\sqrt{\text{m}}\right)\exp\left(0.019\max\left[0;\frac{T_\delta - T_{WP}}{10\ \text{MPa}}\right]\right) \tag{7}$$

This equation is based on Wallin [29], but both Wallin and BS 7910 [1] use a location parameter of 20 MPa$\sqrt{\text{m}}$ instead of 30 MPa$\sqrt{\text{m}}$ in Eq. (7). However, 20 MPa$\sqrt{\text{m}}$ is inconsistent with the relationship between temperature and fracture toughness adopted elsewhere in BS 7910 (e.g. [1], Eqs. K.17 and L.13) and the studies on which this relationship is based (e.g. [37–39]). Therefore the location parameter is adopted as 30 MPa$\sqrt{\text{m}}$ in this work. The Beremin-based crack tip constraint correction and the Master curve apply to lower shelf (cleavage) and transition (from cleavage to ductile) behaviour. For this reason, the T-stress corrections according to Eqs. (6) or (7) are not applied here if the CTOD test result was reported as δ_m, i.e. if it failed after reaching the maximum force.

Following the weakest link concept for cleavage fracture, the constraint-corrected fracture toughness is further corrected for the length of the crack front in case the CTOD test was not reported as δ_m:

$$K^c_{mat} = 20\ \text{MPa}\sqrt{\text{m}} + \left(K^c_{matB} - 20\ \text{MPa}\sqrt{\text{m}}\right)\left(\frac{B_\delta}{l}\right)^{1/4} \tag{8}$$

$$l = \min(l_{cf}, l_{max}) \tag{9}$$

where l_{cf} is the length of the crack front over which the stress intensity factor is approximately equal to the maximum value. It is equal to $2B$ for centre cracked specimen or double edge notch specimen and it is approximated as $2c$ for semi-elliptical cracks [1]. The crack front length is maximized here, associated with the plane strain fracture toughness K_{IC}:

$$l_{max} = 2.5\left(\frac{K_{IC}}{s_y}\right)^2 = 2.5\left(\frac{20\ \text{MPa}\sqrt{\text{m}} + (K^c_{mat} - 20\ \text{MPa}\sqrt{\text{m}})\left(\frac{25\ \text{mm}}{l_{max}}\right)^{1/\lambda}}{s_y}\right)^2 \tag{10}$$

Eqs. (8)–(10) need to be solved iteratively. Note that BS 7910 applies the crack front length correction of Eq. (8) without considering a maximum.

The Mode I stress intensity factor is determined as:

$$K_I = Ys\sqrt{\pi a} + K_{sb,max} \tag{11}$$

where K_{sb} is the stress intensity factor due to the residual stress evaluated from a pre-determined peak value. Alternatively, the self-balancing component of the residual stress field can be employed for surface breaking flaws [1], but the differences between these two alternatives are negligible for the database used here. The product between the geometric correction factor Y and the applied stress s is:

$$Ys = f_w(M_{km}M_m s_m + M_{kb}M_b s_b) + M_m s_{m,res} + M_b s_{b,res} \tag{12}$$

where M are component correction factors, subscripts $_m$ and $_b$ refer to membrane and bending loading, subscript $_{res}$ refers to residual stress (values given later), and subscript $_k$ refers to the geometric influence of weld detail. Parameter f_w accounts for the finite width of a specimen, which is obtained from the parametric equations in BS 7910 [1]. The same applies to the correction factors M_m and M_b, except for full thickness cracks at the edge of a hole, for which [1] does not provide an equation. Various equations for M_m are given in the literature [40–44], with insignificant differences for the crack length over hole diameter ratio that are applied in the tests in Section 3. Bowie's solution [40] is applied in this paper:

$$M_m = \phi_2\sqrt{\sec\left(\pi\frac{D+2a}{4W}\right)} \tag{13}$$

$$\phi_2 = 1 - 0.15\left(\frac{D}{D+2a}\right) + 3.46\left(\frac{D}{D+2a}\right)^2 - 4.47\left(\frac{D}{D+2a}\right)^3 + 3.52\left(\frac{D}{D+2a}\right)^4 \tag{14}$$

where D is the diameter of the hole and W is the specimen width. Factors M_k are taken from the three-dimensional solution in BS 7910 [1], following [45], but they are adjusted for the weld flank angle by multiplying this solution by a factor f_ψ [46]:

$$f_\psi = \begin{cases} \left(10\frac{a}{B}\right)^{-0.5log(A_\psi)} & \text{if } a/B \le 0.1 \\ 1 & \text{if } a/B > 0.1 \end{cases} \tag{15}$$

$$A_\psi = 13.096 \cdot 10^{-3} + 28.199 \cdot 10^{-3}\psi - 139.45 \cdot 10^{-6}\psi^2 \quad (25 \le \psi \le 65) \tag{16}$$

where ψ is 180 minus the weld flank angle in degrees.

The fracture ratio follows from:

$$K_r = K_I / K^c_{mat} + \rho \tag{17}$$

where ρ accounts for plasticity interaction effects between applied load and residual stress. It is taken from the so-called "simplified procedure" in BS 7910 [1].

2.3. Plasticity ratio L_r

The plasticity ratio, L_r, of the WP tests is based on the reference stress estimate:

$$L_r = s_{ref}/s_y \tag{18}$$

where s_{ref} is the reference stress in the wide plate tests, taken from the parametric equations in Annex P of BS 7910 [1]. The equations for the T-stress in the standard also make use of the reference stress, but they are based on different parametric equations for some WP geometries. The reference stress parametric equations in Annex N of [1] are used in those cases. The reference stress in CTOD specimens $s_{ref\delta}$, necessary to determine T_δ in Eq. (7), requires the force at failure of these specimens. These forces are not available for all CTOD tests and they are therefore determined from a fit of the force versus δ data of those CTOD specimens for which this data is available. Using the reference stress equations for single edge notched bend specimens in [1], the fit results in the following relationship between $s_{ref\delta}$ and $K_{mat\delta}$:

$$\frac{s_{ref\delta}}{s_y} = 1.42\exp\left(\frac{-54.3\,\text{MPa}\sqrt{\text{m}}}{K_{mat\delta}}\right) \tag{19}$$

The limit load solution is used to estimate the plasticity ratio of the TJ tests with chord failure [47]:

$$L_r = \frac{s_y + s_u}{2s_y}\left(\left|\frac{P_a}{P_c}\right| + \left(\frac{M_{a,i}}{M_{c,i}}\right)^2 + \left|\frac{M_{a,o}}{M_{c,o}}\right|\right) \tag{20}$$

where P_a, $M_{a,i}$ and $M_{a,o}$ are the applied axial load, in-plane bending moment and out-of-plane bending moment, respectively, and P_c, $M_{c,i}$ and $M_{c,o}$ are their respective plastic resistance counterparts with account of the flaw influence.

A maximum plasticity ratio $L_{r,max}$ applies to both WP and TJ tests:

$$L_{r,max} = \frac{s_y + s_u}{2s_y} \tag{21}$$

The flaw is unacceptable if either the combination (L_r, K_r) is outside the FAL, or if L_r is larger than $L_{r,max}$. BS 7910 [1] provides three options for the description of the FAL. Option 1 is applied here because data required for the other two options are lacking.

3. Test database

3.1. Wide Plate (WP) tests

The test database contains 82 WP tensile tests. Some of the specimens consist of base metal only and others contain welds with the crack in the centre of the weld or in the Heat Affected Zone (HAZ). The WP database contains centre cracked specimens in tension (CCT), specimens containing a hole (diameter 200 mm) with two cracks emanating from that hole (HCCT), surface cracked specimens in tension (SCT), surface cracks in plates with welded cover plates around the weld (CSCT), cruciform joints with curved plates with surface cracks at the weld toe (CJSCT), curved plates with surface cracks in tension (CPSCT), extended surface cracked specimens in tension (ESCT), and double edge notched specimens in tension (DENT) with a crack in the HAZ very close to the fusion line, see Fig. 3(a). The outer radius of the curved plates of the CPSCT and CJSCT specimens was 356 mm, except for specimen number 2896.1, which had an outer radius of 305 mm. Fig. 3(b) gives the cross-section of each specimen with a close-up of the crack and weld location (if any). All WP specimens except for the CJSCT specimens were notched with electro discharge machining and subsequently fatigue loaded to sharpen the crack tip before the fracture test was undertaken. The CJSCT specimen were fatigue

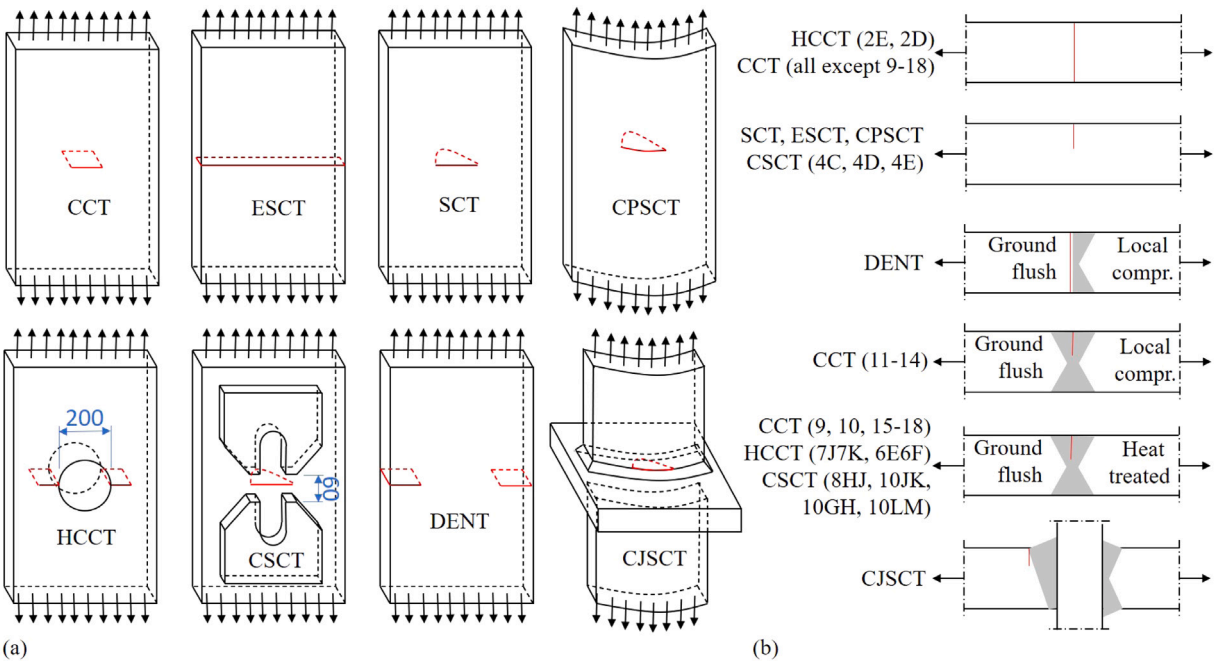

Fig. 3. Wide plate specimen: (a) Specimen types; (b) Cross-section with crack (red) relative to weld (grey), if any.

tested from their as-welded state up to fracture. The crack dimensions at the onset of the fracture test – a as the length of full thickness edge cracks, $2a$ as the length of full thickness centre cracks, a as the depth of surface cracks and $2c$ as the length of surface cracks – were determined from the fracture surface after each test. The tests are reported in [48–54] and the relevant data are summarized below.

Table 1 gives the data of all specimens, where P_u is the load at failure and 'Batch' refers to the material batch from which the specimens were composed, see Table 2. Some specimens exhibited plastic deformation upon reaching P_u. The strain at failure is not reported. Table 2 also provides the temperatures at which the WP and CTOD tests were carried out. The standard tensile tests on base or weld metal of some of the batches were carried out at room temperature, and Table 2 gives the adjusted values at test temperature using Eqs. (2) and (3). Between one and eight CTOD tests were carried out per batch, and Table 2 gives the CTOD values (δ) for each batch. The CTOD specimens were locally compressed according to the standard BS 7448-2 applicable at the time of execution (superseded by ISO 15653 [55]). The loading rates of the CTOD and WP specimens were approximately equal. Care has been taken that the direction of the notch relative to the rolling direction in the CTOD tests matches the crack growth direction in the WP tests. Separate sets of CTOD tests were carried out for the depth and the surface directions for the specimens with a surface crack. In all surface cracked specimens, K_r in depth direction appeared higher than that of the surface direction and therefore Table 2 gives the data for the depth direction.

All WP specimens except for the DENT specimens originated from steel grade Fe510 (various qualities) with a nominal yield stress of 355 MPa. Steel grade FeE550 with a nominal yield stress of 550 MPa was used for the DENT specimens of batch 25–32. The steel grades of the DENT specimens of batches 33–35 are not reported. Failure of all listed WP tests was characterized as unstable.

3.2. Tubular Joint (TJ) tests

Four TJ tests are available in addition to the WP tests, with two configurations (denoted as (a) and (b)) and main dimensions according to Fig. 4. Each of these configurations was tested twice, see the final rows of Table 1. The specimens were pre-fatigued from the as-welded state (i.e. without applying an artificial notch) prior to the fracture test. The TJ specimens were from steel grade Fe510 with a nominal yield stress of 355 MPa.

The failure assessment of a flawed TJ should be based on the hot-spot stress [58]. Linear elastic finite element models are made to determine the Stress Concentration Factors (SCF) and the ratio between membrane and bending stress at the crack location of the two types of TJ specimen [56,57]. The specimens are modelled in ANSYS with linear solid elements with full integration of type SOLID45. The region of interest is modelled with 5 mm cube elements (7 to 9 elements over the chord wall thickness B). The weld profile is modelled with penetration values according to the construction drawings. Linear extrapolation to the weld toe from the surface points of $1.0B$ and $0.4B$ away from the weld toe [59] is applied to determine the hot-spot stress at the locations 1 to 3 or 1 to 5, as indicated in the right pictures of Fig. 4(a) and (b), respectively. The SCF are determined as the ratio between this hot-spot stress and the nominal stress, the latter determined from the forces and full cross-sectional area. Linearization of the stress over

Table 1
WP and TJ tests.

Code	Type	Notch loc.	Batch	B [mm]	W [mm]	a [mm]	c [mm]	P_u [kN]
1	CCT	Base	1	30.3	643	72		6150
2	CCT	Base	2	30.3	648	72		7250
9	CCT	Weld	3	28.2	650	73		6150
10	CCT	Weld	4	27.6	650	73.5		4500
11	CCT	Weld	5	57.7	552	55		12 500
12	CCT	Weld	6	56.1	552	56.5		10 700
13	CCT	Weld	7	56.4	551	58.5		10 800
14	CCT	Weld	8	56.0	551	58.5		10 900
15	CCT	Weld	9	58.0	496	52.5		9250
16	CCT	Weld	10	57.6	552	57.5		11 000
17	CCT	Weld	11	58.6	552	56.5		10 500
18	CCT	Weld	12	57.7	546	56.5		11 700
6B	CCT	Base	13	30.3	650	53.9		8050
2B	CCT	Base	13	29.9	650	27.2		9200
1C	CCT	Base	13	29.9	649	15.9		9650
6A	CCT	Base	14	30.3	651	51.7		7950
2A	CCT	Base	14	29.9	651	27		8250
1A	CCT	Base	14	30.0	649	13.8		8800
6C	CCT	Base	15	30.3	650	53.8		8300
2C	CCT	Base	15	30.0	650	27		9800
1B	CCT	Base	15	30.0	649	13.7		11 000
2E	HCCT	Base	13	30.0	650	9.25		4850
2D	HCCT	Base	14	30.0	650	9.45		6100
6D	HCCT	Base	15	30.0	650	9.1		5950
7J/7K	HCCT	Weld	16	30.0	650	9.1		5550
6E/6F	HCCT	Weld	17	30.0	649	9.45		6000
7L/7M	HCCT	Weld	18	30.0	650	11.35		5800
1D	SCT	Base	19	30.0	651	10.1	23.0	9750
1E	SCT	Base	20	30.0	651	10.1	24.4	11 800
3C	SCT	Base	19	30.0	650	8.7	42.5	9061
3D	SCT	Base	20	30.0	650	9.2	42.5	8385
3E	ESCT	Base	19	30.0	651	7.9		7095
3G	ESCT	Base	20	30.0	651	8.3		7651

(*continued on next page*)

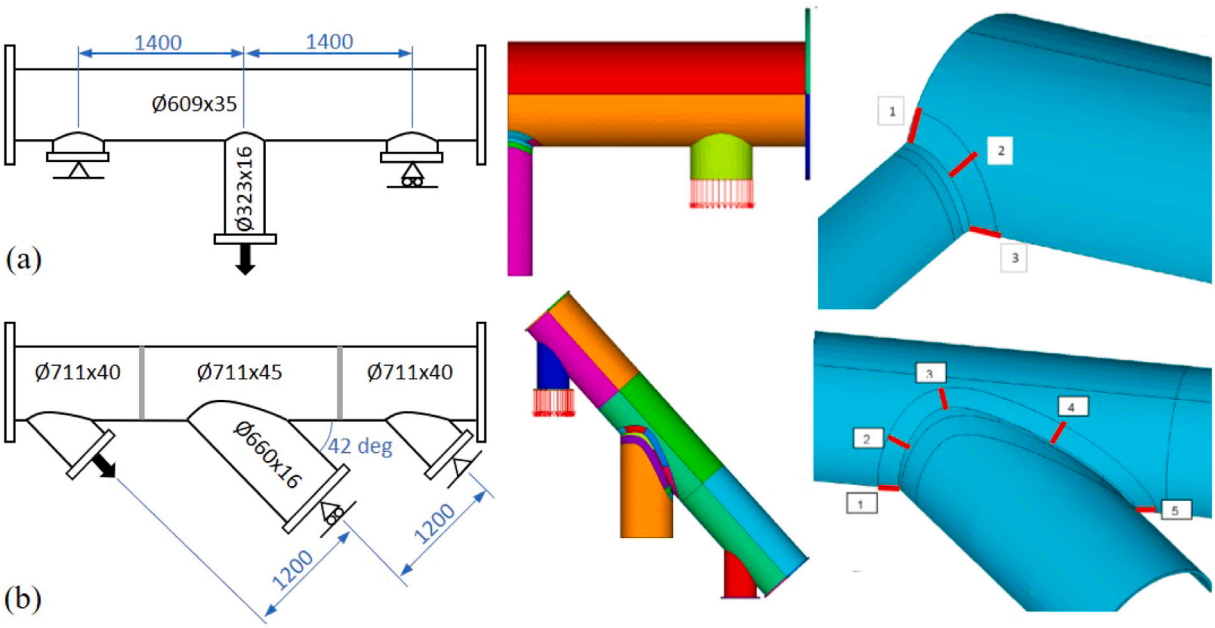

Fig. 4. Tubular joint specimen (dimensions in mm, figures of the finite element method from [56,57]): (a) Specimens BB2 and BB6; (b) Specimens B and D.

Table 1 (*continued*).

Code	Type	Notch loc.	Batch	B [mm]	W [mm]	a [mm]	c [mm]	P_u [kN]
3H	ESCT	Base	19	30.0	650	10.4		5427
3J	ESCT	Base	20	30.0	650	12.9		5362
999.1	CJSCT	HAZ	21	45	139	19.2	57.5	1626
999.2	CJSCT	HAZ	21	45	124	19	52.5	1507
999.3	CJSCT	HAZ	21	45	110	17	37.0	1198
999.4	CJSCT	HAZ	21	45	119	13.3	41.0	1449
601.2	CPSCT	Base	22	45	373	3.5	24.0	7640
601.3	CPSCT	Base	22	45	375	15.2	75.0	5660
2896.1	CPSCT	Base	23	40	378	15.2	75.5	7480
4D	CSCT	Base	20	29.8	648	9.3	42.9	7807
10JK	CSCT	Weld	17	30.9	646	16.7	50.6	7704
10LM	CSCT	Weld	24	30.3	646	11.78	44.4	8678
4C	CSCT	Base	20	29.8	649	8.45	21.7	7692
10GH	CSCT	Weld	24	30.5	650	9.26	21.7	6824
4E	CSCT	Base	20	30.2	648	9.02	20.9	8896
10NO	CSCT	Weld	17	30.2	650	9.04	20.5	11 141
8HJ	CSCT	Weld	24	30.5	650	8.76	21.7	9032
125	DENT	HAZ	25	12.1	175	5.43		1319
127	DENT	HAZ	25	12.2	175	4.32		1297
123	DENT	HAZ	25	12.1	175	17.92		1159
122	DENT	HAZ	25	12.1	175	17.62		1172
126	DENT	HAZ	26	12.1	175	6.14		1326
128	DENT	HAZ	26	12.2	174	5.07		1367
124	DENT	HAZ	26	11.9	175	17.51		1091
121	DENT	HAZ	26	12.1	175	17.34		1203
353	DENT	HAZ	27	40.9	173	4.08		4370
352	DENT	HAZ	27	40.3	173	5.49		4364
355	DENT	HAZ	27	39.9	174	18.14		3563
356	DENT	HAZ	27	40.4	173	16.66		3604
354	DENT	HAZ	28	41.0	173	4.98		3939
357	DENT	HAZ	28	37.5	174	5.32		4126
351	DENT	HAZ	28	40.2	174	17.67		3784
358	DENT	HAZ	28	37.6	175	17.56		3310
359	DENT	HAZ	28	38.0	175	18.89		3210
3510	DENT	HAZ	28	37.9	175	18.96		3594
221	DENT	HAZ	29	37.7	175	17.68		3577
222	DENT	HAZ	29	37.7	175	17.61		3623
223	DENT	HAZ	30	37.8	176	17.65		3609
224	DENT	HAZ	30	37.8	175	17.40		3564
106-1	DENT	HAZ	31	10.0	175	12.64		937
106-2	DENT	HAZ	31	10.0	175	12.51		927
14-1	DENT	HAZ	32	9.6	175	12.12		893
14-2	DENT	HAZ	32	10.6	175	12.52		1033
101-1	DENT	HAZ	33	29.2	171	12.74		3288
101-2	DENT	HAZ	33	29.0	175	12.42		3492
102-1	DENT	HAZ	34	29.3	175	13.29		3928
102-2	DENT	HAZ	34	29.8	175	13.14		3720
460-1	DENT	HAZ	35	45.7	176	13.35		3884
460-2	DENT	HAZ	35	47.7	175	13.31		3821
B	TJ(b)	HAZ	36	45	2000	9.0	124	9000
D	TJ(b)	HAZ	37	45	2000	9.1	42.5	5000
BB2	TJ(a)	HAZ	38	35.7	1120	13.30	197	4050
BB6	TJ(a)	HAZ	39	35.0	1120	9.74	197	2760

the wall thickness at the location of the weld toe (giving the same normal force and bending moment per unit length as the actual stress) is applied to determine the ratio between the membrane and bending stress. Table 3 provides the SCF and the membrane to bending stress ratio resulting from the simulations. The hot-spot stress and the tensile to bending stress ratio follow directly from the table for the deepest point of the crack at the hot spot. Quadratic interpolation using the tabulated values of the SCF and the tensile to bending stress ratio is applied for the surface point of the cracks.

3.3. Choices made in the assessment and application field

A note in BS 7910 [1] informs that the distance between weld toes, L, in evaluating M_k may be reduced to $0.5B$ if the assessment is based on the hot-spot stress. This is adopted in the assessment of the TJ tests. Cracks were inserted in the centre of the weld in the CCT, HCCT and CSCT specimens (Fig. 3(b)) and the weld was ground flush in the DENT and the CPSCT specimens. Factor M_k is therefore taken as unity for these geometries. A linear elastic finite element model consisting of solid elements is made to determine the SCF in the CSCT specimens. Even though the purpose of the cover plates was to generate a stress concentration – with an SCF

Table 2
Tensile test properties and CTOD values.

Batch	θ [°C]	Zone	LP	s_y [a] [MPa]	s_u [a] [MPa]	B [mm]	W [mm]	a/W	δ (results individual tests) [b] [mm]
1	−30	Base	Yes	416	586	30	60	0.5	0.31 0.23
2	−50	Base	Yes	436	605	30	60	0.5	0.20 0.23
3	−30	Weld	No	408 498	557 658	30	30	0.3	0.27 0.31 0.32
4	−55	Weld	No	434 524	580 686	30	30	0.3	0.09 0.11 0.11
5	10	Weld	No	375 506	525 705	60	60	0.3	0.54 0.58 (0.58)
6	−10	Weld	No	390 521	540 725	60	60	0.3	(0.08) (0.19) (0.21) 0.16 0.22 0.23
7	−30	Weld	No	408 539	557 747	60	60	0.3	(0.05) 0.05 0.07
8	−50	Weld	No	428 559	575 772	60	60	0.3	0.06 0.03
9	−10	Weld	No	390 486	540 667	60	60	0.3	0.74 0.82 0.86 0.88 0.94 0.94
10	−30	Weld	No	408 504	557 688	60	60	0.3	0.58 1.06
11	−50	Weld	No	428 524	575 711	60	60	0.3	0.24 0.39
12	−70	Weld	No	453 549	596 737	60	60	0.3	0.09 0.14
13	−70	Base	Yes	460	648	30	60	0.5	0.086 0.11 0.14 0.22 0.36
14	−40	Base	Yes	425	613	30	60	0.5	0.21 0.73 0.93
15	−25	Base	Yes	412	598	30	60	0.5	0.56 0.82 0.86 2.1
16	−70	Weld	No	460 573	648 682	30	60	0.5	0.061 0.075 0.128 0.188
17	−40	Weld	No	425 546	613 652	30	60	0.5	0.35 0.46 0.63
18	−25	Weld	No	412 538	598 640	30	60	0.5	0.43 0.46 0.57 0.58 0.65 0.91 1.27 1.57
19	−70	Base	Yes	460	648	30	30	0.3	0.37 0.37 0.63 0.63 0.67 0.75 0.82 0.86
20	−40	Base	Yes	425	613	30	30	0.32	0.56 1.19 1.31 1.33 1.44 1.47 1.57 1.57
21 [d]	0	HAZ	No	315 [c]	535 [c]	30	30	0.3	0.06 0.08 0.13
22	0	Base	No	325	550	30	30	0.3	0.06 0.09 0.09 0.11 0.11 0.12
23	0	Base	No	427	593	30	30	0.3	0.22 0.25 0.32 0.39 0.52 0.74
24	−70	Weld	Yes	460 573	648 682	30	30	0.3	0.45 0.52 0.83
25	−10	HAZ	Yes	590 653	702 725	12	24	0.5	0.065 0.15 0.21
26	−30	HAZ	Yes	607 670	723 747	12	24	0.5	0.065 0.24 0.26
27	20	HAZ	Yes	546 640	618 666	40	82	0.5	0.15 0.14 0.18 0.76 0.29
28	−10	HAZ	Yes	567 662	644 694	40	82	0.5	0.12 0.04 0.16 0.26 0.12
29	20	HAZ	Yes	546 660	618 728	40	75	0.5	0.57 0.21 0.67 0.15 0.18 0.35 0.20
30	−10	HAZ	Yes	567 682	644 759	40	76	0.5	0.05 0.20 0.21 0.36 0.38 1.02
31	−25	HAZ	Yes	537 554	658 623	10	20	0.5	0.28 0.28
32	−10	HAZ	Yes	579 531	676 659	10	19	0.5	0.08 0.19
33	10	HAZ	No	731 775	840 842	30	58	0.5	0.06 0.11
34	−10	HAZ	No	844 819	923 888	30	59	0.5	0.15 0.09
35	−40	HAZ	Yes	484 570	587 683	46	91	0.5	0.72
36	0	HAZ	No	308 [c]	530 [c]	44	45	0.3	0.07 0.31 0.21
37	0	HAZ	No	308 [c]	530 [c]	44	45	0.3	0.08 0.27 0.11
38	0	HAZ	No	354 [c]	540 [c]	35	36	0.3	0.83 1.11 1.39
39	0	HAZ	No	302 [c]	550 [c]	34	35	0.3	0.38 0.45 0.58

[a] If two values are given, first value is for Base metal, second value is for Weld metal.
[b] Underlined values are δ_m. Values between brackets are from tests with $W = 2B$ and $a/W = 0.5$ (deviating from the other tests in the batch).
[c] Values are for Base metal. Weld metal was overmatched.
[d] WP and CTOD tests are from one delivery with the same composition and texture, but possibly from different batches.

Table 3
SCF and ratio membrane to bending stress in the TJ specimens.

Specimen type	Stress location	SCF	s_m/s_b
Fig. 4(a)	1	2.83	0.30
Fig. 4(a)	2	2.75	0.52
Fig. 4(a)	3	2.56	1.07
Fig. 4(b)	1	3.41	0.87
Fig. 4(b)	2	2.40	0.84
Fig. 4(b)	3	0.31	1.68
Fig. 4(b)	4	0.41	0.85
Fig. 4(b)	5	0.57	3.52

of more than 2 reported in the original documentation – the results of the model indicate that the cover plates did not result in an appreciable stress concentration at the location of the crack and thus M_k is set to unity for this specimen type. An average of the measured angles ψ (180 minus the weld flank angle in degrees) is reported equal to 25.7, 32.5 and 25.7 for the CJSCT, TJ(a) and TJ(b) specimens, respectively, and these values are adopted in Eq. (16).

Table 4
Residual stress applied in the assessment of the specimens containing welds.

Specimen type	$s_{m,res}/s_y$	$s_{b,res}/s_y$	$K_{sb,max}/s_y$	Section of [1]
CJSCT	0.5	$(0.5-a/B)$	0	Q.4.2
DENT, CCT(11-14)	0.311	0	0	Q.2.2[(a)]
HCCT, CSCT, TJ(b), CCT(9,10,15-18)	0.2	0	0	7.1.10.3
TJ(a)	0.496	$(0.216-0.432\frac{a}{B})$	$0.21\sqrt{B}$	Q.5

[(a)]Different from [1], $s_{b,res}$ and $K_{sb,max}$ are taken as 0 to reflect local compression of these specimens.

BS 7910 [1] does not give parametric equations for the T-stress of cracks emanating from a hole. A three-dimensional finite element model consisting of solid elements was therefore created of the HCCT specimens. Based on the outcome, the T-stress is estimated as −0.65 times the reference stress. This is slightly less negative than the T-stress of a central crack with crack length $2a+D$. The equation parameters accounting for crack tip constraint or T-stress in BS 7910 [1] are not compatible with the equations that consider strength mismatch between base and weld metal [60,61]. Strength mismatch assessment equations have therefore not been used in the current work. Instead, K_r is determined with the material properties of the metal containing the crack (weld metal or base metal), whereas L_r is determined with the minimum of the yield stress of the weld metal and that of the base metal. This selection considers the local and global nature of the fracture and plasticity-induced failure modes, respectively.

For surface cracked WP specimens, BS 7910 [1] provides reference stress solutions for hinge-supported specimens and for specimens with normal restraint against out-of-plane bending. The solutions for normal restraint are used here, reflecting the restraint against out-of-plane bending exerted by the clamps in the test set-up.

The residual stress depends on the type of weld and the weld procedure. BS 7910 [1] provides guidance on the residual stress to be assumed in the assessment. Table 4 gives the membrane and bending portions and the maximum stress intensity factor related to the selfbalancing component of the residual stress, $s_{m,res}$, $s_{b,res}$ and $K_{sb,max}$, respectively, as assumed in the assessment for the different types of specimen. HCCT, CSCT specimens containing welds, TJ(b) specimens, and CCT specimens 9, 10, and 15–18 were post weld heat treated and a reduced residual stress then applies. BS 7910 [1] does not give guidance for the residual stress in full through thickness cracks that are locally compressed prior to testing, as in case of DENT specimens and CCT specimens 11–14. The membrane residual stress is assumed equal to that of a butt joint according to [1], whereas the bending residual stress and the self-balancing stress are assumed zero for these specimens. This estimate is selected as an intermediate value between the measured residual stresses after warm prestressing in [62] and the residual stress of through thickness flaws without treatment in [1].

The database consists of (predominantly) uniaxially loaded specimens. Pressure vessels are not part of the database, and data in [7] suggest that particularly the bias of L_r is larger for pressured cylinders as compared to wide plates with the BS 7910 [1] assessment procedure. Similarly, WP tests subject to biaxial loading in [62] show a larger scatter as compared to uniaxially loaded tests. Hence, the results in this paper are limited to uniaxial in-plane loaded steel components.

4. Probabilistic model

A radial distance d_i between the FAL and the failure point (L_r, K_r) for each test i is defined as:

$$d_i = r_{F,i} - r_{FAL,i} \tag{22}$$

where $r_{FAL,i}$ and $r_{F,i}$ are the radial distances of the FAL and of the test failure point, respectively, from the origin. The polar angle ϕ_i for $r_{FAL,i}$ is taken equal to that of the failure point, see Fig. 5 for an example. Two main probabilistic models are considered with two variants for each. An additive MU, Δ, independent of the polar angle is considered in probabilistic Model 1, where the probabilistic FAL is equal to the deterministic FAL+Δ − 1. Two distributions are considered for d_i, namely, a normal distribution (Eq. (23)) and a two-parameter lognormal distribution, (Eq. (24)).

$$d_i + 1 \sim^{IID} \mathcal{N}(\mu_\Delta, \sigma_\Delta) \tag{23}$$

$$d_i + 1 \sim^{IID} \log\mathcal{N}(\mu_\Delta, \sigma_\Delta) \tag{24}$$

where μ_Δ is the mean and σ_Δ is the standard deviation of Δ, $\mathcal{N}$ is the normal distribution, and superscript ^{IID} refers to independent and identically distributed random variables. The probabilistic formulation is defined such, that the minimum possible value of the probabilistic FAL in case of the lognormal distribution is the deterministic FAL minus 1. The shift of −1 is an approximation that reflects the physics-based fact that L_r and K_r cannot be negative.

Probabilistic Model 2 is similar to Model 1, but the distribution parameters of Δ are polar angle dependent:

$$\mu_\Delta(\phi) = \mu_{\Delta L} + \left(\mu_{\Delta K} - \mu_{\Delta L}\right)\frac{\phi}{\pi/2} \tag{25}$$

$$\sigma_\Delta(\phi) = \sigma_{\Delta L} + \left(\sigma_{\Delta K} - \sigma_{\Delta L}\right)\frac{\phi}{\pi/2} \tag{26}$$

The frequentist paradigm is used to interpret and to estimate the model parameters (μ_Δ and σ_Δ in the first model, $\mu_{\Delta L}$, $\sigma_{\Delta L}$, $\mu_{\Delta K}$ and $\sigma_{\Delta K}$ in the second model) [63]:

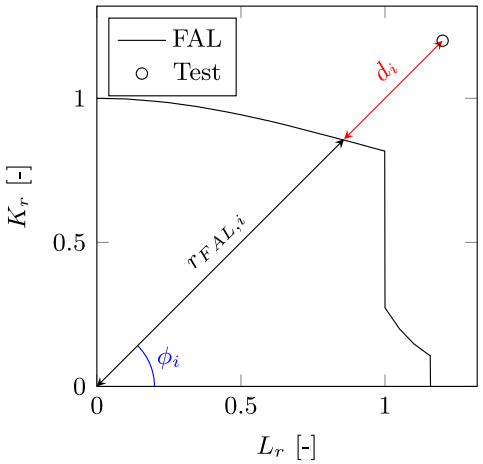

Fig. 5. Example of failed test i with definitions of $r_{FAL,i}$, d_i and ϕ_i.

- The point estimates of the model parameters are obtained by maximizing the likelihood function.
- The standard errors due to sampling variability are estimated using the delta method [64].

The bounds of the 90% CI of the probabilistic FAL – i.e. 5% and 95% one-sided confidence bounds – are subsequently determined from these parameters. The Akaike Information Criterion (AIC) [65] is used to compare the performance of the models with respect to the goodness of model fit observations while penalizing model complexity. Following [66], a difference between two models is considered as significant if the absolute difference in AIC exceeds 10.

5. Results

5.1. All tests combined

This section considers all available WP (or TJ) tests and associated CTOD tests as mutually independent realizations. In each realization, K_{mat} is determined from an individual CTOD test and K_I and s_{ref} are determined from the corresponding WP (or TJ) test. The MU is determined from all of these realizations without considering dependence. Table 5 gives the resulting MU parameters. The first three sets of parameters apply to different treatment of the T-stress namely, no consideration of T-stress, Ainsworth's model (Eq. (6)) and Wallin's shift of the master curve (Eq. (7)). The last set with footnote (a) will be introduced later. The following differences between the options and models apply for the available data:

- Based on the AIC differences, the shifted lognormal distribution gives a consistently and significantly better fit of the data than the normal distribution.
- Based on the AIC differences, the probabilistic Model 2 – where the MU is taken as dependent on the ratio between K_r and L_r – performs consistently and significantly better than Model 1 – where the MU distribution is independent of the assessment points.
- The sets that consider the T-stress have lower standard deviations than the set that ignores the T-stress. In addition, the μ values are closer to 1 for the sets that consider the T-stress. This demonstrates that a more accurate description of reality is obtained by considering the T-stress. For the available data and based on the same indicators, it appears that considering the T-stress through Wallin's shift of the master curve performs similar as the model of Ainsworth.

The dots in subfigures (a) of Figs. 6–8 show d_i of all test data as a function of the normalized polar angle for the three possibilities of treating T-stress. The curves provide the mode (i.e. most frequent value) of the distribution and the 90% CI of the lognormally distributed MU of probabilistic Model 2. Subfigures (b) provide the same data expressed as (L_r, K_r) assessment points, where the curves apply to a sample material with $s_y = 475$ MPa and $s_u = 632$ MPa. Note that these curves are given for demonstration purposes only; each material batch has its own FAL and d_i is determined with that FAL. The curves in subfigures (b) provide the mode and the 90% CI of the lognormal distributed MU of probabilistic Model 1. Comparing the figures, it is obvious that the scatter of data and the related 90% CI reduces substantially if the T-stress is taken into account in K_r.

Fig. 9(a) repeats the data of Fig. 8, but it distinguishes the material zones containing the crack. The data with a notch in the HAZ or in the weld metal have a slightly larger bias and scatter as compared to the data with a crack in the base metal. The larger scatter may be due to the variation of residual stress levels and variation of the microstructure of the HAZ and weld specimens. The larger bias may be related to the consideration of the T-stress in BS 7910 [1]. The standard allows evaluation of the T-stress from primary loading and residual stress but, using the option of the parametric equations in Annex N, it only considers the effect

Table 5
MU considering each combination of WP (or TJ) test and CTOD test.

T-stress correct.	Distr. d_i	Prob. model	AIC	μ_Δ [b] $\mu_{\Delta L}$ [b]	σ_Δ [b] $\sigma_{\Delta L}$ [b]	$\mu_{\Delta K}$ [b]	$\sigma_{\Delta K}$ [b]
None	$\mathcal{N}$	1	269	1.319 (0.018)	0.349 (0.013)		
		2	59	1.072 (0.031)	0.113 (0.015)	1.665 (0.063)	0.509 (0.034)
	$\log\mathcal{N}$	1	148	1.316 (0.016)	0.307 (0.013)		
		2	10	1.073 (0.028)	0.112 (0.015)	1.659 (0.057)	0.479 (0.034)
Eq. (6)	$\mathcal{N}$	1	−69	1.102 (0.011)	0.219 (0.008)		
		2	−197	1.001 (0.016)	0.134 (0.009)	1.406 (0.055)	0.345 (0.032)
	$\log\mathcal{N}$	1	−151	1.101 (0.011)	0.200 (0.008)		
		2	−241	1.005 (0.014)	0.125 (0.009)	1.389 (0.051)	0.345 (0.032)
Eq. (7)	$\mathcal{N}$	1	−87	1.151 (0.011)	0.213 (0.008)		
		2	−175	1.116 (0.021)	0.107 (0.011)	1.213 (0.062)	0.400 (0.033)
	$\log\mathcal{N}$	1	−164	1.150 (0.010)	0.196 (0.008)		
		2	−226	1.120 (0.019)	0.102 (0.011)	1.197 (0.056)	0.375 (0.032)
Eq. (7)[a]	$\mathcal{N}$	1	−290	1.089 (0.008)	0.161 (0.006)		
		2	−372	1.068 (0.017)	0.088 (0.009)	1.130 (0.052)	0.294 (0.026)
	$\log\mathcal{N}$	1	−349	1.089 (0.008)	0.151 (0.006)		
		2	−406	1.073 (0.016)	0.086 (0.008)	1.112 (0.048)	0.281 (0.024)

[a] With Eq. (27) for s_{ref} of surface cracked specimens instead of the BS 7910 [1] equations, and the T-stress based on primary stress and residual stress.
[b] First value is the point estimate, value between parenthesis is the standard error. The mean of the shifted lognormal distribution is $\mu_X - 1$.

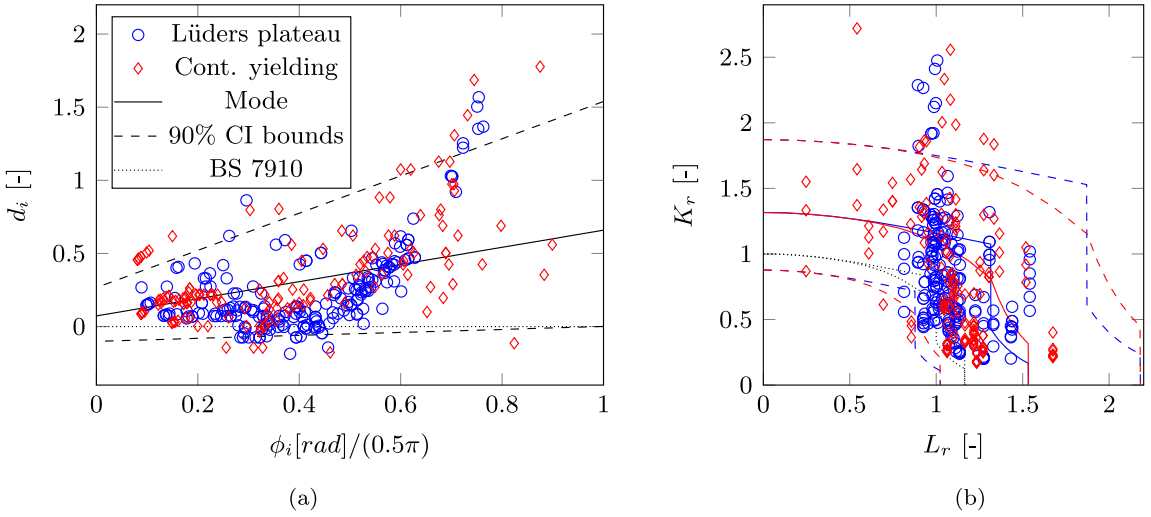

Fig. 6. MU using all data without considering T-stress influence: (a) d_i versus ϕ with probabilistic Model 2; (b) K_r versus L_r with probabilistic Model 1.

of the T-stress caused by primary loading. Yamashita and Minami [31,67] have shown that the residual stress also contributes to the T-stress. Their WP tests were assessed closer to the FAL in case the residual stress is considered in calculating the T-stress.

Fig. 9(b) distinguishes the type of specimen. This appears to have a significant influence on the MU distribution. The surface cracked (SCT, CPSCT, CJSCT and TJ) specimens show a larger bias and a larger scatter as compared to the other types of specimen. This may be (partially) related to the derivation of the equations for the reference stress of surface cracked specimens in BS 7910 [1], in which the surface crack is modelled with a square envelope and where a uni-axial stress state and yield locus are assumed, [68]. Miura and Takahashi [69] collected five possible alternatives from other literature for the reference stress of surface cracked specimens. All alternatives are considered here, and the alternative in [70] gives the best fit in terms of agreement of the MU distribution with the non-surface cracked specimens. The corresponding reference stress follows from:

$$s_{ref} = \frac{s_m}{(1-\zeta)^{0.43}} \tag{27}$$

$$\zeta = \begin{cases} \frac{ac}{B(B+c)} & \text{if } W \geq 2(B+c) \\ \frac{2ac}{BW} & \text{if } W < 2(B+c) \end{cases} \tag{28}$$

The last set of data in Table 5 as well as Fig. 10 present the results considering:

- Eq. (27) for the reference stress of surface cracks.

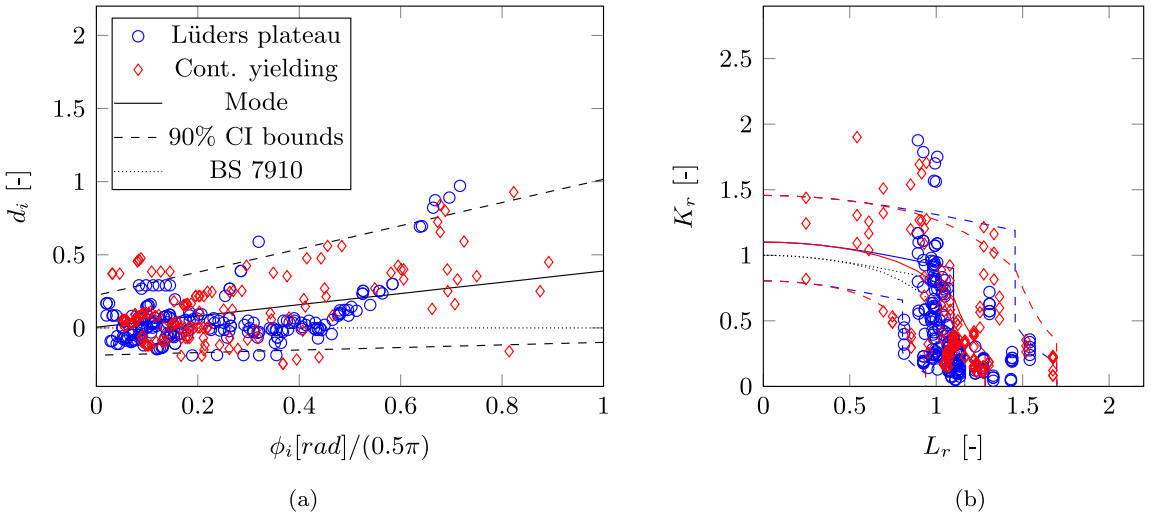

Fig. 7. MU using all data with Ainsworth's T-stress correction, Eq. (6): (a) d_i versus ϕ with probabilistic Model 2; (b) K_r versus L_r with probabilistic Model 1.

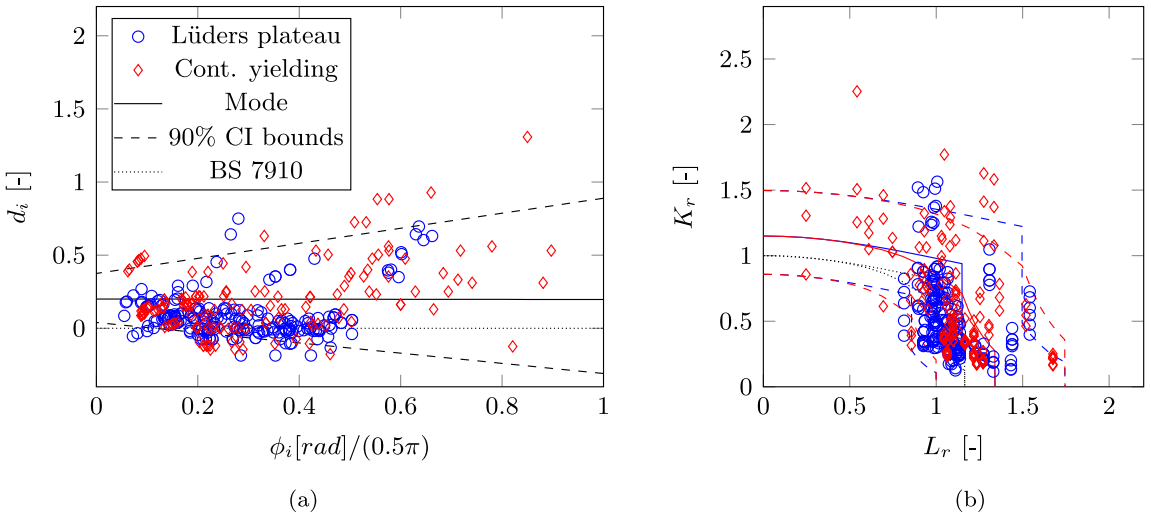

Fig. 8. MU using all data with T-stress shift of the master curve, Eq. (7): (a) d_i versus ϕ with probabilistic Model 2; (b) K_r versus L_r with probabilistic Model 1.

- The T-stress as composed from the contribution of the primary stress and the residual stress and accounting for it using the shift of the master curve.

The values σ being lower and the values μ being closer to 1 show that this gives a more accurate prediction of reality than the other sets.

5.2. Minimum and average of three equivalent (MOTE, AOTE)

The evaluation of the previous section is useful to select the optimal combination of models. In most practical assessments, however, a limited number of K_{JC} or CTOD tests are carried out and the Minimum Of Three Equivalent (MOTE) test results is selected to determine K_r. The term "equivalent" refers to the need that the individual tests give reasonably close fracture toughness values. BS 7910 [1] recommends to consider the fracture toughness as the lower 20th percentile of more than three fracture toughness tests if the crack tip constraint is considered in the assessment. However, this requires prior knowledge on the type of distribution of the fracture toughness, because the number of tests per batch in Table 2 appears too small to select a distribution type based on the data (using the Kolmogorov–Smirnov test or the chi-squared test). The equation for the lower 20th percentile given by the standard results in a fracture toughness close to zero or even negative for a number of specimens when assuming a normal distribution. Deriving the MU from such a database is not meaningful and it is therefore not applied here. To establish the MU from as many

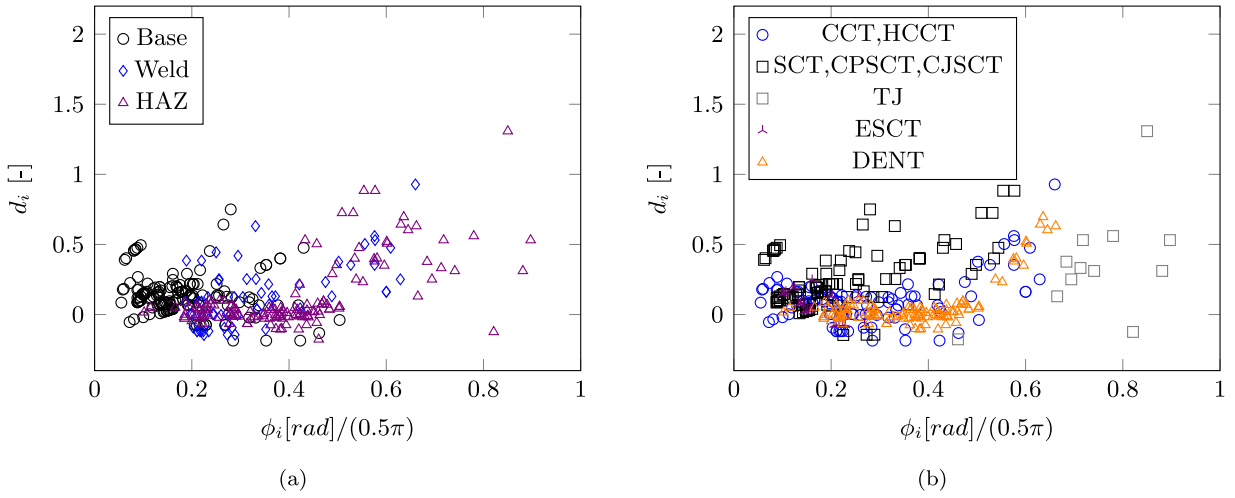

Fig. 9. All data with T-stress shift of the master curve, Eq. (7): (a) Different metallic zones; (b) Different geometries.

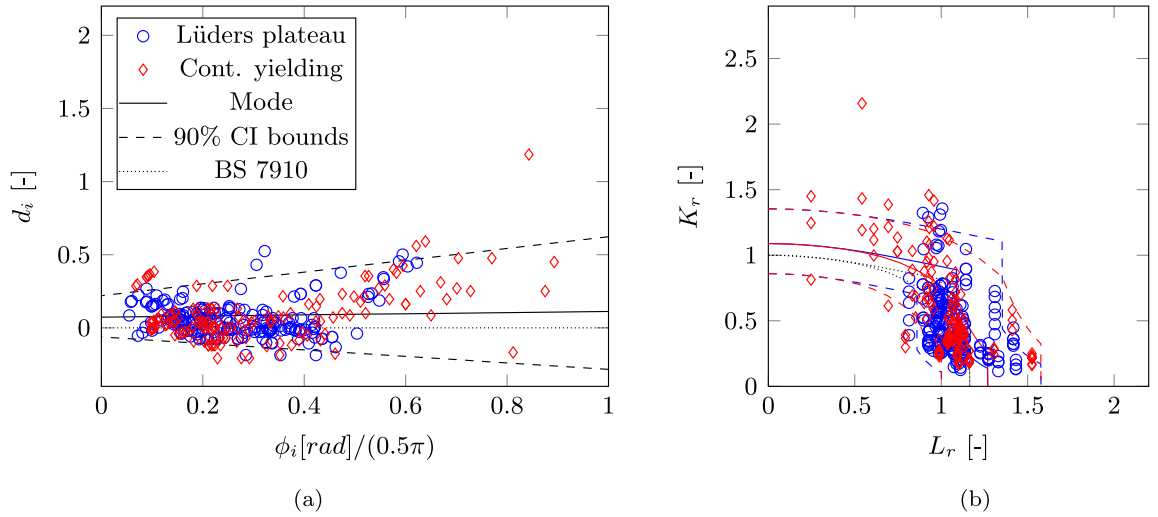

Fig. 10. MU using all data with T-stress based on primary and residual stress, considered through the shift of the master curve, Eq. (7), and reference stress for surface cracked specimen according to Eq. (27): (a) d_i versus ϕ with probabilistic Model 2; (b) K_r versus L_r with probabilistic Model 1.

available data as possible, using consistency in the number of fracture toughness tests, and to be of use also in practical cases with a limited number of fracture toughness tests, the MU is evaluated here using three CTOD tests per specimen, by a procedure outlined below, even if more CTOD tests are available. BS 7910 [1] specifies that an individual test value should neither be smaller than 70% nor larger than 140% of the average of three to be "equivalent". Otherwise, more tests need to be carried out. This practice is applied to the WP and TJ test database as follows:

- Tests from batches with less than three CTOD data are ignored.
- Sampling without replacement is used of CTOD data with more than three specimens per batch. The sample of three is accepted if it satisfies the "equivalent" criterion.
- Re-sampling is applied if the sample of three is not accepted.
- In case the "equivalent" criterion is not met even after 100 times re-sampling, the three values closest to the mean of the batch are taken as the sample.

The minimum per sample of three equivalent is used to determine K_{mat} in the assessment for MOTE. In addition, the Average Of Three Equivalent (AOTE) tests is selected, which is defined as the arithmetical mean of the fracture toughness values of three equivalent tests.

To account for sampling uncertainty in the above described procedure, a total of 100 databases are generated using the bootstrap method (i.e. with re-sampled specimens), where each database contains all WP and TJ tests and three sampled "equivalent" CTOD

Table 6
MU using three CTOD tests per WP (or TJ) test (shifted lognormal distribution).

T-stress correct.	Selection CTOD	Prob. model	AIC	μ_Δ [(b)] $\mu_{\Delta L}$ [(b)]	σ_Δ [(b)] $\sigma_{\Delta L}$ [(b)]	$\mu_{\Delta K}$ [(b)]	$\sigma_{\Delta K}$ [(b)]
None	MOTE	1	56	1.457 (0.044)	0.367 (0.036)		
		2	25	0.952 (0.088)	0.147 (0.051)	2.021 (0.125)	0.442 (0.076)
	AOTE	1	11	1.308 (0.031)	0.261 (0.024)		
		2	−2	1.056 (0.068)	0.145 (0.046)	1.651 (0.110)	0.355 (0.075)
Eq. (6)	MOTE	1	−8	1.162 (0.027)	0.228 (0.021)		
		2	−30	1.006 (0.036)	0.123 (0.025)	1.513 (0.104)	0.358 (0.073)
	AOTE	1	−42	1.091 (0.021)	0.178 (0.016)		
		2	−46	1.015 (0.032)	0.136 (0.025)	1.301 (0.094)	0.262 (0.075)
Eq. (7)	MOTE	1	2	1.234 (0.029)	0.245 (0.023)		
		2	−15	1.099 (0.058)	0.101 (0.034)	1.445 (0.131)	0.418 (0.078)
	AOTE	1	−35	1.154 (0.022)	0.186 (0.017)		
		2	−40	1.130 (0.044)	0.100 (0.028)	1.191 (0.115)	0.349 (0.074)
Eq. (7)[(a)]	MOTE	1	−30	1.158 (0.023)	0.194 (0.017)		
		2	−48	1.055 (0.053)	0.092 (0.026)	1.329 (0.120)	0.309 (0.060)
	AOTE	1	−71	1.091 (0.017)	0.144 (0.013)		
		2	−75	1.095 (0.039)	0.082 (0.021)	1.066 (0.105)	0.264 (0.056)

[(a)] With Eq. (27) for s_{ref} of surface cracked specimens instead of the BS 7910 [1] equations, and the T-stress based on primary stress and residual stress.
[(b)] First value is the point estimate, value between parenthesis is the standard error.

Table 7
FAL safety factor required for a 5% lower confidence bound for three CTOD tests per WP (or TJ) test.

T-stress correction	None	Eq. (6)	Eq. (7)	Eq. (7)[(a)]
MOTE	1.06	1.21	1.14	1.15
AOTE	1.08	1.21	1.19	1.15

[(a)] With Eq. (27) for s_{ref} of surface cracked specimens instead of the BS 7910 [1] equations, and the T-stress based on primary stress and residual stress.

values per test. The MU parameters are evaluated from these 100 databases for the MOTE and the AOTE, assuming a lognormal distribution for $d_i + 1$. Table 6 gives the resulting MU parameters: for each parameter the mean of the 100 estimates. Obviously, the scatter of the samples and the 90% CI are smaller for AOTE in comparison to MOTE, due to the greater confidence in the mean as compared to a lower bound based on three CTOD tests. The L20P appears to give the largest scatter of the three alternatives for K_{mat}.

Based on a limited number of WP tests, Hadley [28] suggests that the FAL can give unconservative results for an assessment using MOTE and considering the T-stress influence in the assessment. Pisarski [32] and Hadley and Pisarski [34] indicate that, if accounting for the T-stress, a more rigorous definition for the lower bound fracture toughness may be required instead of MOTE to determine K_r. This is confirmed with the current analysis, see Fig. 11, which shows the resulting MU distribution and the data of one of the 100 database realizations as an example. A non-negligible number of tests are within the FAL. The figure also shows that the confidence interval is largest for L20P (subfigure (c)) and smallest for AOTE (subfigure (d)), with MOTE (subfigure (b)) in between these two options.

The distribution parameters of Table 6 allow the estimation of the fraction of test data that exceeds the FAL. Using probabilistic Model 1, the FAL corresponds to the 8% lower confidence bound if K_{mat} is based on MOTE and the T-stress is not considered. This fraction is 25% or 17% for the T-stress considered through Eq. (6) or Eq. (7), respectively. A division factor to the FAL can be introduced with a value such that the assessment corresponds to a certain, desired lower confidence bound. Fig. 12 gives the relationship between the confidence bound and the safety factor and, as an example, Table 7 gives the safety factors required to achieve a 5% lower confidence bound. The safety factor can be implemented in practical assessments either by dividing the FAL with the factor, or by vectorial multiplication of the (L_r, K_r) coordinate with it. The first option corresponds to the lower confidence bound displayed in Fig. 11.

The Appendix of this paper evaluates the MU using all available CTOD tests instead of the three used in this section. The safety factors appear relatively close to the ones given in Table 7.

6. Discussion and application examples

6.1. Remarks about the MU estimate

The MU established in the previous section contains the uncertainty of the fracture toughness as based on a limited number of CTOD tests. Strictly, the distribution derived is hence not only a MU but it is a combination of the true uncertainty of the assessment procedure and the uncertainty of the true fracture toughness. This is underlined by the fact that the scatter in all models is lowest for low values of $\phi/(0.5\pi)$, where the plasticity (which is typically more deterministic) is dominant. The coefficient of variation for

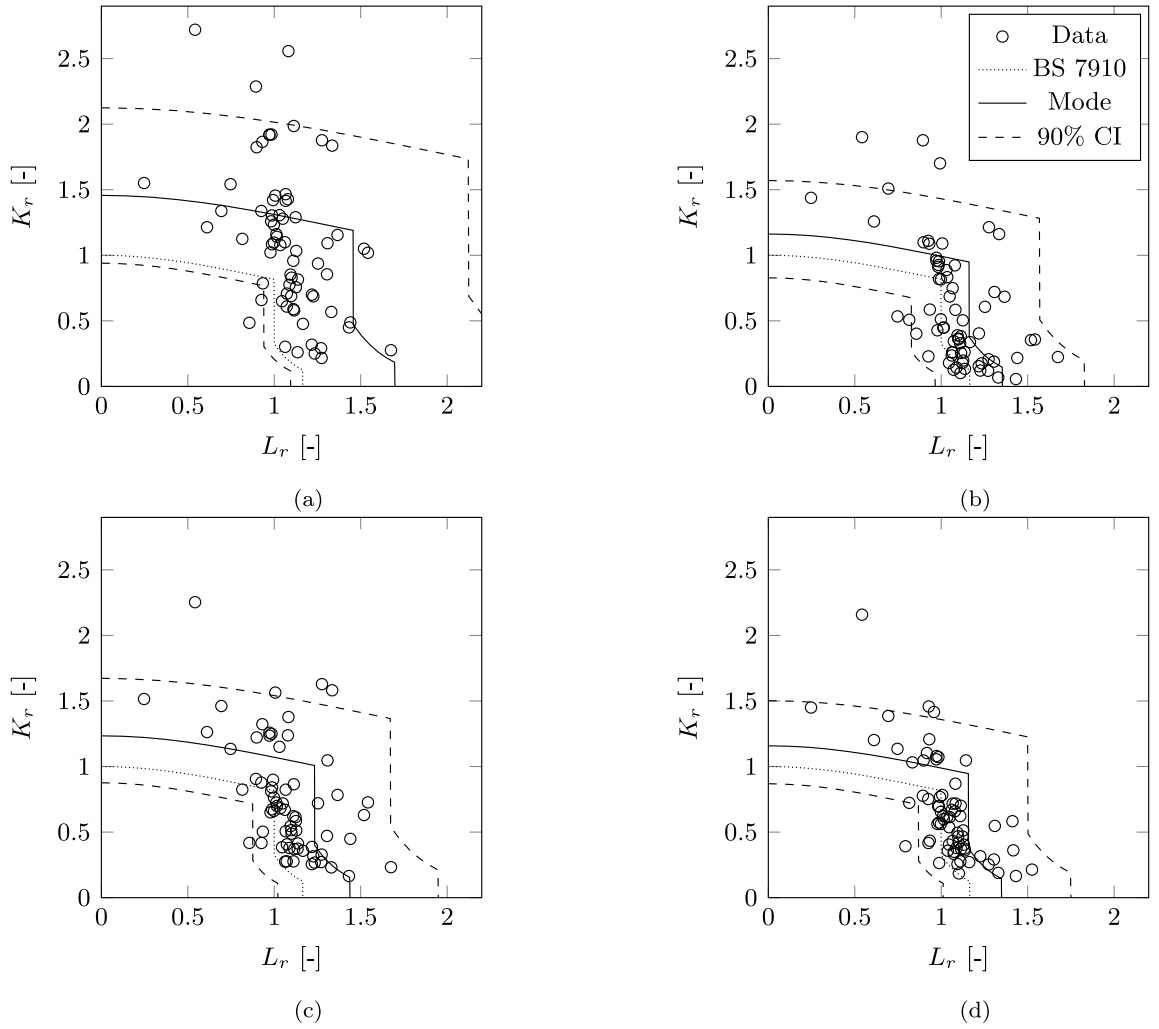

Fig. 11. MU for MOTE with probabilistic Model 1: (a) Without T-stress correction; (b) Eq. (6); (c) Eq. (7); (d) Eq. (7) using primary stress and residual stress and Eq. (27) for s_{ref} of surface cracked specimens.

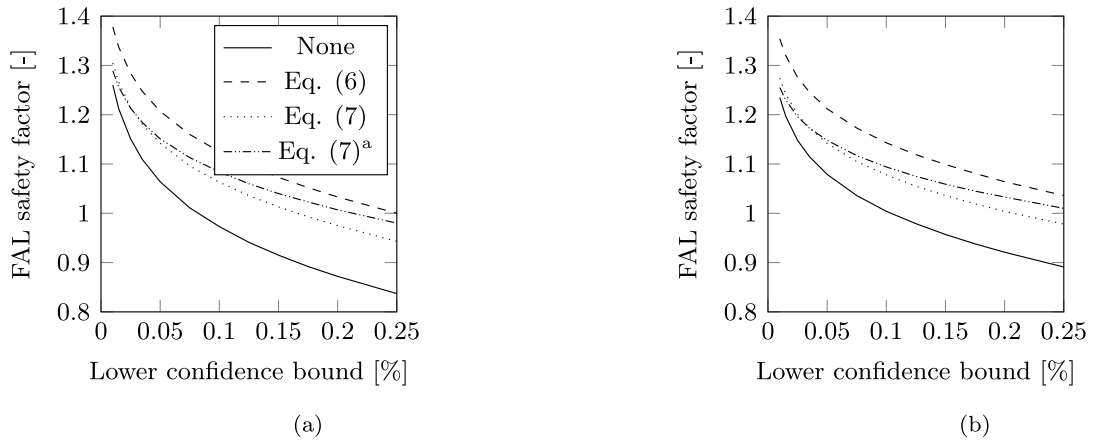

Fig. 12. Required safety factor for a desired lower confidence bound: (a) MOTE; (b) AOTE.

a base metal batch estimated from 106 tests was 0.41 in [32] and it was 0.43 for a batch estimated from 20 tests in [71]. Both sets comprise of steel specimens and contain a mix of ductile and brittle data. In order to estimate the contribution of the uncertainty in K_{mat}, a lognormal distribution is considered for K_{mat} as in [34], with a coefficient of variation of 0.41. Sets of three samples are randomly selected from that distribution and the MOTE and AOTE are determined for each set for which the criterion of equivalence is met. This is repeated until 500 MOTE and AOTE values are obtained. The coefficient of variation of the 500 MOTE values is 0.27 and that of the AOTE values is 0.25. Comparing these values with the values of $\sigma_{\Delta K}$ in Table 6, it appears that a large fraction of the scatter can be explained by the uncertainty of K_{mat}. Possible causes for the remaining scatter are: variations in the residual stress in the CTOD and the WP (and TJ) tests, the complexity of geometries of the WP tests versus the nominal geometry applied in the model (such as the assumption of semi-elliptical crack shapes for surface cracks), and the multitude of material zones in the tests versus the assumption of homogeneous material for the assessment of the T-stress influence and for the effect of the crack front length, l, on the fracture toughness (Eq. (9)).

The bias and scatter in L_r are attributed to the complexity of some of the geometries and to possible influence of the T-stress on the Von Mises or Tresca yield load, whereas most parametric equations for s_{ref} are based on a uniaxial stress state. As a demonstration, the figures indicate that both bias and scatter in L_r are smaller for the DENT specimens as compared to other specimen types. Indeed, the equations for s_{ref} of the DENT specimens are detailed in that these consider possible weld mismatch and plane strain versus plane stress state, [72]. Moreover this specimen type is not subject to out-of-plane bending. The bias in L_r is smaller than the bias determined in older studies, such as those of Fig. 2. This is partially due to the availability of reference stress solutions for more types of geometry in the current version of BS 7910 [1], see the comparison in [7]. The additional difference could be related to the assumption of restraint of the specimen. Normal restraint against out-of-plane bending is assumed in the current paper, whereas it is possible that a more conservative pin restraint was assumed in other studies.

Considering the T-stress influence through the master curve shift, Eq. (7) gives a comparable model performance as Ainsworth's model, Eq. (6). This may be a consequence of the database, where most large scale tests failed around $L_r = 1$. This was also the starting point of the derivation of the master curve shift in [29]. Indeed, the master curve shift model performs worse for the test data with large polar angles. Tronskar et al. [30] show that the accuracy of Wallin's original T-stress consideration (i.e. Eq. (7) with 20 instead of 31 MPa$\sqrt{\text{m}}$) depends on the steel grade.

Hadley and Pisarski [34] suggest that the FAL with T-stress consideration according to Eq. (7) could still be used if a lower bound value different than MOTE is used for $K_{mat\delta}$. This approach has two drawbacks. First, it would require many more than three K_{JC} or CTOD tests, and second, as more accurate estimates of L_r become available and hence the level of conservatism in L_r reduces (but some scatter remains), some of the test data with small polar angle ϕ will fall inside the FAL, as is evident from Fig. 10. A very low value of $K_{mat\delta}$ is then required to get these data outside the FAL. Instead, the authors of the current paper consider it advantageous to apply (or enlarge) a safety factor on the FAL, as given in Fig. 12 or Table 7. Because of the higher confidence of the mean than of a lower bound value in case of a limited number of test data, it may then also be better to base the assessment and the safety factor on the AOTE instead of the MOTE.

The data in subfigures (a) of Figs. 6–8 and 10 show a distinct non-linear dependency on the polar angle that is in conflict with the assumed statistical model. As an approximation, the authors accept this conflict and cover this seemingly non-random pattern with a single random variable (the MU), however, this should be analysed in further studies. The difference between the figures implies that a more accurate base model ([1] and T-stress effect in this study) could largely eliminate the pattern and in turn could make the residuals more resemble a random sample from a (log)normal distribution.

6.2. Application Example 1: use of MOTE and AOTE

Consider a plate in an existing structure with a stress relieved butt weld and with dimensions $B = 25$ mm, $W = 1000$ mm, distance between weld toes $L = 40$ mm and weld toe angle = 150 degrees. A weld toe flaw is present with $a/c = 0.5$. The plate is of steel grade S355, for which [73] provides the following distributions of the material properties at room temperature:

- Shifted lognormal distribution for s_y with a shift of 325 MPa, $\mu_{s_yRT} = 394$ MPa and $\sigma_{s_yRT} = 25$ MPa.
- Shifted lognormal distribution for s_u with a shift of 461 MPa, $\mu_{s_uRT} = 566$ MPa and $\sigma_{s_uRT} = 25$ MPa.
- A correlation coefficient between s_y^{RT} and s_u^{RT} of 0.6 applies.

In addition, the yield stress distribution is truncated at its lower tail at 355 MPa in order to reflect the acceptance tests carried out by steel manufacturers for this steel grade. The design temperature is −30 °C and the (50-year maximum) applied tensile stress is Gumbel distributed with an expectation of 200 MPa and a coefficient of variation of 0.1:

$$F(s) = exp(-exp(-\alpha_1(s-\alpha_2))) \tag{29}$$

where $F(s)$ is the cumulative distribution function of the applied stress s and α_1 and α_2 are the distribution parameters with values of 0.064 and 191 MPa, respectively. The residual stress after stress relief is assumed as $s_{res,m} = 0.2s_y$. A material batch is considered with the true fracture toughness (from deeply notched three-point bending tests) being lognormal distributed with $\mu_{Kmat\delta} = 100$ MPa $\sqrt{\text{m}}$ and $\sigma_{Kmat\delta} = 40$ MPa $\sqrt{\text{m}}$. However, this distribution is unknown and instead, three CTOD tests are executed. Hence, three values are randomly selected from the distribution. The values are 82, 103 and 73, MPa $\sqrt{\text{m}}$, i.e. MOTE = 73 MPa$\sqrt{\text{m}}$ and AOTE = 86 MPa $\sqrt{\text{m}}$. The probability is considered that a flaw with depth a results in failure. The limit state function is:

$$g = r_{FAL,i} + d_i - r_{F,i} \tag{30}$$

Table 8
Distribution of material properties of old mild steel bridges at $\theta = -30\,°C$ [75].

X	Number of samples	Distr. type	μ_X	σ_X
s_y	239	$\log\mathcal{N}$	307 MPa	33 MPa
s_u	243	$\log\mathcal{N}$	446 MPa	39 MPa
$K_{mat\delta}$	195	$\log\mathcal{N}$	125 MPa $\sqrt{\text{m}}$	85 MPa $\sqrt{\text{m}}$

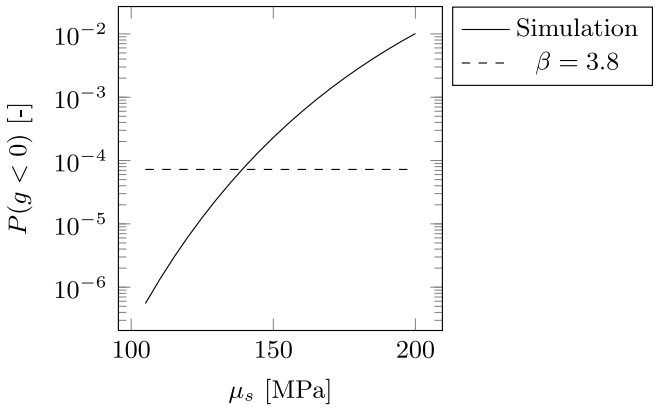

Fig. 13. Results of Example 2: probability of failure as a function of the expectation of the applied 50-year maximum tensile stress.

The distributions of s, s_y and s_u and the procedures of Section 2 are used in determining $r_{F,i}$. The T-stress is considered through Eq. (7) and the corresponding distribution parameters μ_Δ and σ_Δ according to Table 6 (i.e. no dependency is considered on ϕ) are used for d_i (note that μ_Δ and σ_Δ are different for MOTE and AOTE).

ISO 13822 [74] recommends a minimum reliability index of $\beta = 3.8$ with a reference period of 50 years for an existing structure with medium consequences of failure. This implies that the tolerable probability of not obtaining the limit state is:

$$P(g < 0) = \Phi(-\beta) = 3 \cdot 10^{-4} \tag{31}$$

where Φ is the cumulative standard normal distribution. The first order reliability index is employed to estimate the crack depth a that just satisfies the requirement. It is $a = 0.22B$ for MOTE and $a = 0.30B$ for AOTE. The assessment is repeated 100 times, each time sampling three equivalent $K_{mat\delta}$ values from the distribution. AOTE resulted in a larger tolerable flaw than MOTE in all repetitions. The average critical crack depth of the 100 repetitions is $a = 0.22B$ for MOTE and $a = 0.29B$ for AOTE. This example demonstrates the added value of basing the assessment on AOTE instead of MOTE.

6.3. Application Example 2: flaw in an existing bridge

Many mild steel bridges built before the Second World War are still in use to date. Charpy impact or other fracture toughness tests were not carried out in the construction industry at the time of construction. In order to obtain material data of such old bridges, samples from approximately 50 European bridges built between 1870 and 1938 were collected in a European research and tensile tests and K_{JC} tests were carried out on the samples, [75]. Table 8 provides the distributions of the material properties gained from that research at a temperature of −30 °C.

Fatigue cracks can initiate from rivet holes in these structures. After reaching a certain size, the stress intensity factor of such cracks is similar to that of a crack emanating from a hole without a rivet, if the joint contains multiple rivets. A two-sided through-thickness flaw is assumed in such a joint in an old mild steel bridge. It is inspected with magnetic particle inspection. Based on the information in [76], the probability of detection as a function of the flaw size a_d is considered here as Weibull distributed with a location parameter of 0.25 mm, a shape parameter of 0.7 and a scale parameter with a point estimate of 1.2 mm and a standard error of 0.7 mm. Herein, a_d is the detected crack size outside of the rivet head. According to information in [77], the distance between the edge of the rivet head and the edge of the rivet hole (i.e. rivet head radius minus rivet hole radius) of the often applied rivet with shaft diameter of 24 mm is approximately $a_r = 9$ mm. The probability is determined of the crack being detected before failure of the joint. The limit state function is the same as in Example 1, Eq. (30), but $r_{FAL,i}$ is evaluated for a crack with size $a = a_d + a_r$ and d_i is taken from the MU of the FAL using all specimens, i.e. Table 5, using the set of Eq. (7), lognormal distribution for Δ, and probabilistic Model 1. The (50-year maximum) applied stress is Gumbel distributed with a coefficient of variation of 0.1 and a mean that is varied. The first order reliability method is applied to solve the reliability problem as a function of the mean of the maximum applied tensile stress μ_s. Results are presented with the solid curve in Fig. 13. The dashed horizontal line represents the required reliability β as in Example 1. The tolerable mean of the distribution of the applied tensile stress distribution joint is $\mu_s = 140$ MPa (see Fig. 13).

Table A.9
MU using all available CTOD tests per WP (or TJ) test (shifted lognormal distribution).

T-stress correct.	Selection CTOD	Prob. model	AIC	μ_{Δ} [(b)] $\mu_{\Delta L}$ [(b)]	σ_{Δ} [(b)] $\sigma_{\Delta L}$ [(b)]	$\mu_{\Delta K}$ [(b)]	$\sigma_{\Delta K}$ [(b)]
None	MOTE	1	70	1.516 (0.049)	0.407 (0.040)		
		2	31	0.919 (0.090)	0.149 (0.047)	2.142 (0.125)	0.460 (0.071)
	AOTE	1	10	1.318 (0.031)	0.260 (0.024)		
		2	−3	1.063 (0.069)	0.146 (0.045)	1.659 (0.109)	0.345 (0.072)
Eq. (6)	MOTE	1	8	1.185 (0.031)	0.258 (0.024)		
		2	−21	0.998 (0.036)	0.113 (0.026)	1.585 (0.113)	0.429 (0.082)
	AOTE	1	−43	1.092 (0.021)	0.177 (0.016)		
		2	−47	1.017 (0.032)	0.136 (0.026)	1.298 (0.092)	0.255 (0.075)
Eq. (7)	MOTE	1	9	1.263 (0.031)	0.259 (0.024)		
		2	−11	1.072 (0.060)	0.113 (0.037)	1.562 (0.127)	0.403 (0.079)
	AOTE	1	−38	1.159 (0.022)	0.183 (0.016)		
		2	−41	1.125 (0.044)	0.104 (0.029)	1.219 (0.111)	0.329 (0.073)
Eq. (7)[(a)]	MOTE	1	−25	1.182 (0.024)	0.200 (0.018)		
		2	−47	1.014 (0.053)	0.110 (0.028)	1.471 (0.108)	0.272 (0.058)
	AOTE	1	−72	1.091 (0.017)	0.143 (0.013)		
		2	−76	1.101 (0.038)	0.081 (0.02)	1.053 (0.102)	0.261 (0.054)

[(a)] With Eq. (27) for s_{ref} of surface cracked specimens instead of the BS 7910 [1] equations, and the T-stress based on primary stress and residual stress.
[(b)] First value is the point estimate, value between parenthesis is the standard error.

Table A.10
FAL safety factor required for a 5% lower confidence bound using all available CTOD tests per WP (or TJ) test.

T-stress correction	None	Eq. (6)	Eq. (7)	Eq. (7)[(a)]
MOTE	1.05	1.23	1.13	1.13
AOTE	1.07	1.21	1.19	1.15

[(a)] With Eq. (27) for s_{ref} of surface cracked specimens instead of the BS 7910 [1] equations, and the T-stress based on primary stress and residual stress.

7. Conclusions

This paper estimates the MU of the FAL by comparing the assessment according to the British Standard BS 7910:2019 with the actual failure load of 82 WP tensile tests and 4 TJ tests. The following conclusions are drawn:

1. The bias and the scatter of the MU reduce substantially if the crack tip constraint is taken into account.
2. Irrespective of whether or not the T-stress is considered – and how – a non-negligible number of WP specimens has a lower failure load than the one predicted by the FAL, if based on three fracture toughness tests. Depending on the selected assessment procedure, the FAL coincides with the 13% to 25% lower confidence bound if $K_{mat\delta}$ is based on MOTE and the T-stress is considered in the assessment.
3. Instead of using MOTE, a better agreement with the tests and a less conservative assessment results if AOTE is taken as a basis for the assessment, together with an associated error distribution of the FAL (which is obviously different for AOTE compared to MOTE).
4. Instead of using more than three equivalent fracture tests to determine a more rigorous value of the lower bound fracture toughness, as proposed by others if the T-stress is considered, it is advantageous to apply (or enlarge) a safety factor on the FAL. See Table 7 for the required safety factors in case of a 5% lower confidence bound.
5. The AIC shows that the MU can be described better with a shifted lognormal distribution as compared to a normal distribution.
6. The assessment procedure in BS 7910 can be (further) improved by considering the residual stress field in estimating the T-stress from the compendium in Annex N and, for surface flaws, by providing a more accurate description of the reference stress.

CRediT authorship contribution statement

Johan Maljaars: Validation, Methodology, Investigation, Formal analysis, Writing – original draft. **Árpád Rózsás:** Investigation. **Carey L. Walters:** Writing – review & editing. **Henk Slot:** Writing – review & editing.

Declaration of competing interest

The authors declare that they have no known competing financial interests or personal relationships that could have appeared to influence the work reported in this paper.

Acknowledgements

Rijkswaterstaat is acknowledged for the financial support of this study. Monica Nicoreac is acknowledged for collecting a part of the test data from old reports. PT Structural is acknowledged for producing the finite element models of the tubular joints.

Appendix. Evaluation with MOTE and AOTE from all available CTOD tests

Section 5 gave the MU distribution for the case where three CTOD tests are selected for each WP or TJ test. BS 7910 [1] provides guidance to the selection of the fracture toughness if more than three CTOD tests are available. The MOTE is the lowest fracture toughness following from three to five CTOD specimens or the second lowest following from six to ten CTOD specimens. This appendix gives the MU distribution using this guidance, where each WP or TJ test is evaluated using the full set of CTOD specimens (between three and eight depending on the batch). The AOTE is also determined using the full set of CTOD specimens. Table A.9 gives the evaluation of the MU, assuming a lognormal distribution for $d_i + 1$. Table A.10 gives the safety factor required for a 5% lower confidence bound as derived from the MU. Because the number of CTOD tests available is different for the different batches, the evaluation provided here is database dependent and it should be used with caution in case of an assessment in practice. On the other hand, the distributions and required safety factors are close to those evaluated with three CTOD tests in Tables 6 and 7.

References

[1] BS 7910:2019. Guide to methods for assessing the acceptability of flaws in metallic structures. BSI; 2019.
[2] API 579:2016. Recommended practice for fitness-for-service. API; 2016.
[3] R6:2001. Assessment of the integrity of structures containing defects. revision 4. EDF Energy; 2001.
[4] Hadley I. BS 7910:2013 In brief. Int J Press Vessels Pip 2018;165:263–9.
[5] Hadley I, Lei Y. Outline of the fracture clauses of BS 7910:2013. Int J Press Vessels Pip 2018;168:289–300.
[6] Wiesner CS, Maddox SJ, Xu W, Webster GA, Burdekin FM, Andrews RM, Harrison JD. Engineering critical analyses to BS 7910—the UK guide on methods for assessing the acceptability of flaws in metallic structures. Int J Press Vessels Pip 2000;77:883–93.
[7] Kouzoumis K, Hadley I, Mostafavi M. Validation of BS 7910 fracture assessment procedures; wide plates and cylinders. Int J Press Vessels Pip 2021;190:104309.
[8] Maljaars J, Steenbergen HMGM, Vrouwenvelder ACWM. Probabilistic model for fatigue crack growth and fracture of welded joints in civil engineering structures. Int J Fatigue 2012;38:108–17.
[9] Jutla T, Garwood SJ. Interpretation of fracture toughness data. Met Constr 1987;5:276–81R.
[10] Burdekin FM, Hamour W. Partial safety factors for SINTAP procedure. Health and Safety Executive; 2002.
[11] Hadley I, Wu G. Treatment of reliability in fracture assessments using BS 7910 Annex K. Int J Press Vessels Pip 2018;168:310–22.
[12] Dijkstra OD. A fracture mechanics approach to the assessment of the remaining fatigue life of defective welded joints. In: Proceedings of IABSE 1990. 1991, p. 1–12.
[13] PD 6493:1980. Guidance on methods for assessing the acceptability of flaws in fusion welded structures. BSI; 1980.
[14] Joint Committee of Structural Safety. JCSS probabilistic model code. JCSS; 2021, https://www.jcss-lc.org/jcss-probabilistic-model-code/.
[15] Muhammed A, Pisarski HG, Stacey A. Using wide plate test results to improve predictions from probabilistic fracture mechanics. In: 13 th European conference on fracture. ECF; 2000, p. 6–9.
[16] PD 6493:1991. Guidance on Methods for assessing the acceptability of flaws in fusion welded structures. BSI; 1991.
[17] Kocak M, Webster S, Janosch JJ, Ainsworth RA, Koers R. FITNET fitness-for-service (FFS). GKSS Research Centre; 2008.
[18] Muhammed A. Background to the derivation of partial safety factors for BS 7910 and API 579. Eng Fail Anal 2007;14:481–8.
[19] Hadley I, Wiesner CS, Maddox SJ. PD 6493 Becomes BS 7910; what's new in fracture and fatigue assessment? In: I Mech E seminar Flaw assessment in pressure equipment and welded structures. 1999.
[20] (institutional authors). SINTAP structural integrity assessment procedures for european industry. European Commission; 1999.
[21] Du Z-Z, Hancock JW. The effect of non-singular stresses on crack-tip constraint. J Mech Phys Solids 1991;39(4):555–67.
[22] Betegón C, Hancock JW. Two-parameter characterization of elastic-plastic crack-tip fields. ASME J Appl Mech 1991;58:104–13.
[23] Minami F, Ohata M, Shimanuki H, Handa T, Igi S, Kurihara M, Kawabata T, Yamashita Y, Tagawa T, Hagihara Y. Method of constraint loss correction of CTOD fracture toughness for fracture assessment of steel components. Eng Fract Mech 2006;73:1996–2020.
[24] Minami F, Ohata M. Constraint assessment of brittle fracture of steel components, iso 27306 vs. FITNET FFS. Eng Fract Mech 2012;84:67–82.
[25] Beremin FM, Pineau A, Mudry F, Devaux J-C, D'Escatha Y, Ledermann P. A local criterion for cleavage fracture of a nuclear pressure vessel steel. Metall Trans A 1983;14A:2277–87.
[26] ISO 27306:2016. Metallic materials — method of constraint loss correction of CTOD fracture toughness for fracture assessment of steel components. 2016.
[27] Ainsworth RA, O'Dowd NP. Constraint in the failure assessment diagram approach for fracture assessment. J Press Vessel Technol 1995;117:260–7.
[28] Hadley I, Horn A. Treatment of constraint in BS 7910: 2013, ISO 27306 and DNVGL-RP-f108. Int J Press Vessels Pip 2019;169:77–93.
[29] Wallin K. Quantifying Tstress controlled constraint by the master curve transition temperature T0. Eng Fract Mech 2001;68:303–28.
[30] Tronskar JP, Mannan MA, Lai MO. Accounting for constraint effects in fracture mechanics analysis of floating production, storage and off-loading vessels and ships. Eng Fract Mech 2002;69:1219–48.
[31] Yamashita Y, Minami F. Constraint loss correction for assessment of CTOD fracture toughness under welding residual stress–part II: Application of toughness correction methodology. Eng Fract Mech 2010;77:2419–30.
[32] Pisarski H. Treatment of fracture toughness data for engineering critical assessment (ECA). Weld World 2017;61:723–32.
[33] Slatcher S. Estimation of characteristic values of fracture toughness. J Test Eval 1990;18:141–59.
[34] Hadley I, Pisarski H. Materials properties for engineering critical assessment: Background to the advice given in BS 7910:2013. Int J Press Vessels Pip 2018;168:191–9.
[35] Seal CK, Sherry AH. Predicting the effect of constraint on cleavage and ductile fracture toughness using area contour toughness scaling. Eng Fract Mech 2017;186:347–67.
[36] Rice JR, Tracey DM. On the ductile enlargement of voids in triaxial stress fields. J Mech Phys Solids 1969;17:201–17.
[37] Wallin K. Master curve analysis of ductile to brittle transition region fracture toughness round robin data – the "EURO" fracture toughness curve. VTT; 1998.
[38] Wallin K. The master curve method: a new concept for brittle fracture. Int J Mater Prod Technol 1999;14:342–54.

[39] ASTM E1921-10. Standard test method for determination of reference temperature, T0, for ferritic steels in the transition range. American Society for Testing and Materials; 2010.
[40] Bowie OC. Analysis of an infinite plate containing radial cracks originating from the boundary of an internal circular hole. J Math Phys 1956;35:60–71.
[41] Tada H, Paris PC, Irwin GR. The stress analysis of cracks handbook. 3rd ed.. ASME Press; 2000.
[42] Murakami Y, Keer LM. Stress intensity factors handbook, vol. 3. J Appl Mech 1993;60:1063.
[43] Newman I, Raju I. Stress intensity factor equations for cracks in three-dimensional finite bodies subjected to tension and bending loads, Vol. 85. NASA Technical Memorandum; 1984, p. 1–38.
[44] Waldman W. Beta factors for collinear asymmetrical cracks emanating from an offset circular hole in a rectangular plate. Defence Science and Technology Group Fishermans Bend Victoria Australia; 2016.
[45] Bowness D, Lee MMK. Fracture mechanics assessment of fatigue cracks in offshore tubular structures, 2000/077. Health and Safety Exectutive; 2002.
[46] Dijkstra OD, Snijder HH, Straalen IJ. Fatigue crack growth calculations using stress intensity factors for weld toe geometries. In: International conference on offshore mechanics and arctic engineering OMAE 1989. 1989, p. 1–7.
[47] (Institutional author). Offshore technology report 015-2001. health and safety executive; 2002.
[48] Ter Avest FJ, Lont MA, Wildschut H. Small scale test and wide plate test evaluation in relation to brittle fracture in welded structures EUR 9434 EN. Commission of the European Communities; 1985.
[49] Van Rongen HJM. Verslag van breukanalyses op RWS componenten met de revisie van PD 6493. TNO; 1989.
[50] Van Rongen HJM, H. W. Breukanalyses uitgevoerd op 23 NIL- "wide plate" proefstukken met behulp van de revisie van PD 6493. 1990.
[51] Van Rongen HJM, H. W. Fracture analysis of 10 wide plate specimens with slot plates and with a surface defect on the basis of the CEGB R6 failure assessment method and the revision of PD 6493. TNO; 1990.
[52] Van Rongen HJM, H. W. Fracture analysis of 3 pre-fatigued large scale tubular Y-nodes from coarse grained material. TNO; 1990.
[53] Van Rongen HJM. Breukanalyses op tien wide plates uit het onderzoek: verwerkbaarheid van HRS. TNO; 1993.
[54] Ter Avest FJ, Dahl W, Vuik J, Delede F. Influence of local brittle zones on the fracture behaviour of welded joints in a steel with a minimum yield of 550 MPa. Commission of the European Communities; 1997.
[55] ISO 15653:2018. Metallic materials – method of test for the determination of quasistatic fracture toughness of welds. ISO; 2018.
[56] Gaida A, van Damme DJ. TNO T Pipe connection hotspot weld, 16009B02. PT Structural design and analysis; 2017.
[57] Gaida A, van Damme DJ. TNO Y Pipe connection hotspot weld, 16009B01. PT Structural design and analysis; 2017.
[58] Burdekin FM. The fracture behaviour of a welded tubular joint–an ESIS TC1-3 round robin on failure assessment methods: Part III-UK bs7910 methodology. Eng Fract Mech 2002;69:1119–27.
[59] Karamanos SA, Romeijn A, Wardenier J. Stress concentrations in tubular gap K-joints: mechanics and fatigue design. Eng Struct 2000;22:4–14.
[60] Lei Y, Ainsworth RA. A j integral estimation method for cracks in welds with mismatched mechanical properties. Int J Press Vessels Pip 1997;70:237–45.
[61] Wang Y-Y, Rudland D, Horsley D. Development of a FAD-based girth weld ECA procedure: Part I—Theoretical framework. In: 4th international pipeline conference, Vol. 36207. 2002, p. 1717–26.
[62] Hadley I, London T. Optimising fracture assessment of welded structures using BS 7910, R6 and FEA. In: International conference on offshore mechanics and arctic engineering, OMAE 2019. 2019, p. 1–10.
[63] Rossi RJ. Mathematical statistics : an introduction to likelihood based inference. Wiley; 2018.
[64] Doob JL. The limiting distributions of certain statistics. Ann Math Stat 1935;6:160–9.
[65] Akaike H. Information theory and an extension of the maximum likelihood principle. Springer; 1998, p. 199–213.
[66] Burnham KP. Model selection and multimodel inference. In: A practical information-theoretic approach. 1998.
[67] Yamashita Y, Minami F. Constraint loss correction for assessment of CTOD fracture toughness under welding residual stress. Part I: Methodology using the equivalent ctod ratio. Eng Fract Mech 2010;77:2213–32.
[68] Willoughby AA, Davey TG. Plastic collapse in part-wall flaws in plates. In: 20th ASTM symp. fracture mechanics: perspectives and directions. 1989, p. 390–409.
[69] Miura N, Takahashi Y. Evaluation of J-integral for surface cracked plates under biaxial loading using extended reference stress method. In: 19th int. conf. structural mechanics in reactor technology, SMiRT 19. 2007, p. 1–8.
[70] Sattari-Far I, Dillström P. Local limit load solutions for surface cracks in plates and cylinders using finite element analysis. Int J Press Vessels Pip 2004;81:57–66.
[71] Hadley I, Dawes MG. Fracture toughness testing of weld metal: Results of a European round robin. Fatigue Fract Eng Mater Struct 1996;19:963–73.
[72] Kim Y-J, Schwalbe K-H. Compendium of yield load solutions for strength mis-matched DE (T), SE (B) and C (T) specimens. Eng Fract Mech 2001;68:1137–51.
[73] Melcher J, Kala Z, Holickỳ M, Fajkus M, Rozlívka L. Design characteristics of structural steels based on statistical analysis of metallurgical products. J Construct Steel Res 2004;60:795–808.
[74] ISO 13822:2010. Bases for design of structures – assessment of existing structures. ISO; 2010.
[75] Cremona C, Patron A, Johansson B, Larsson T, Eichler B, Höhler S, Kühn B. Improved assessment methods for static and fatigue resistance of old steel railway bridges – background document D4.6. European Commission 6th framework programme; 2007.
[76] Fahr A, Forsyth D, Bullock M, Wallace W. POD Assessment of NDI procedures-results of a round robin test. In: Review of progress in quantitative nondestructive evaluation. Springer; 1995, p. 2391–8.
[77] Collette Q. Riveted connections in historical metal structures (1840-1940). Hot-driven rivets: technology, design and experiments, Vrije Universiteit Brussel; 2014, http://dx.doi.org/10.13140/2.1.3157.2801.